Sedimentology (2007) **54,** 265–292 doi: 10.1111/j.1365-3091.2006.00834.x

Source-controlled carbonates in a small Eocene half-graben lake basin (Shulu Sag) in central Hebei Province, North China

ZAIXING JIANG*, DAIZHAO CHEN†, LONGWEI QIU‡, HONGBIN LIANG§ and JUN MA§
**College of Energy, China University of Geosciences, #29 Xueyuan Road, Beijing 100083, China (E-mail: jiangzx@cugb.edu.cn)*
†Institute of Geology and Geophysics, Chinese Academy of Sciences, PO Box 9825, Beijing 100029, China
‡Faculty of Earth Resources and Information, Petroleum University, East China, Dongying 257061, Shandong Province, China
§Research Institute of Petroleum Exploration and Development, Huabei Oil Company, China National Petroleum Corporation (CNPC), Renqiu City, Hebei 062552, China

ABSTRACT

Carbonate deposits, which unconformably overlie the Palaeozoic bedrocks, extensively occur in the base of the Tertiary lake succession in the half-graben Shulu Sag, central Hebei Province, North China. This study focuses on the basal carbonate successions on the hinged western slope. Based on seismic, borehole and core data, nine facies are identified in the carbonate successions, and are further grouped into five facies associations: mid-proximal alluvial fan, distal alluvial fan, fan fringe, moderately deep lake and deep lake. The first two facies associations constitute alluvial fans formed by debrisflows at the edge of lake and are dominated by mounded- to lobate-shaped, matrix- to clast-supported carbonate rudstones with minor calcretes in the lowermost rudstone units and basinward increase in interfingering with lacustrine carbonate facies. The fan fringe, moderately deep lake and deep lake associations are dominated by pebbly carbonate arenites (or rare carbonate arenites), calcisiltite-calcilutites, and varve-like calcilutites, calcareous shales and oil shales, respectively. Widespread occurrences of fine-grained limestone packages containing varve-like organic-rich laminations, minor authigenic glauconite and pyrite, and planktonic and plant fossils suggest a meromictic, anoxic deep lake under a semi-humid to humid climate, probably with a connection to marine basins. Similarities in lithology and fossil assemblages (e.g. trilobites) of lithoclasts with those of the Mid-Upper Cambro-Ordovician bedrock carbonates suggest that the clastic and dissolved carbonate loads were sourced from this Lower Palaeozoic catchment, and shed off the surrounding highlands into the basin. These carbonate facies associations represent the lake lowstand and transgressive deposits of the basal third-order sequence (Ia) in which the highstand deposits are composed of lacustrine siliciclastics. During the lake lowstand stage (or initiation of basin-filling) under an intermediate climate, carbonate alluvial fans occurred mostly subaerially at the bottom of the hinged slope with a narrow, shallow lake zone basinwards, and locally were perched within the palaeovalley on the mid-upper slope. During the transgressive (deepening) stage under a semi-humid to humid climate, carbonate alluvial fans became smaller in size and episodically stepped backwards upon the slope, with greatly expanded and deepened lake. Nevertheless, the carbonate system was switched to an exclusively siliciclastic system during the highstand stage. The exhumation and erosion of the Mid-Lower Cambrian bedrock dominated by siliciclastics was probably the cause due to further uplift of the drainage basin. All these facts indicate

that the carbonate deposition in the Shulu Sag was mostly controlled by the interactions of tectonics, climate and provenance.

Keywords Alluvial fan, carbonates, debrisflow, half-graben, lake, North China, Tertiary, varve.

INTRODUCTION

Shulu Sag is a NE–SW trending half-graben (5–10 km wide, ~40 km long) located in the south-western corner of Jizhong (central Hebei) Depression (Zha, 1988; Zhang *et al.*, 2001), a part of the Tertiary Bohai Bay strike-slip rift basins of North China (Fig. 1). These intracontinental rift basins, mostly filled by Tertiary lacustrine deposits with abundant accumulation of organic matter (e.g. Ye *et al.*, 1993), are very important oil-producing basins in China (e.g. Li, 1981; Hellinger *et al.*, 1985; Ye *et al.*, 1985; Zhou *et al.*, 2004). Analogous rift lake basins with comparable tectonic and climatic settings can be found in the modern lakes Tanganyika and Malawi, East Africa (Cohen, 1989, 1990; Scholz & Rosendahl, 1990; Soreghan & Cohen, 1996), and in the Cretaceous Campos basin, offshore Brazil (Abrahão & Warme, 1990).

Lacustrine carbonate deposits are widely reported in the Tertiary lake basins of Bohai Bay area, in which they are mostly of autochthonous origin (i.e. algal buildups, grainstones shoal) (Du, 1990, 1996; Ye *et al.*, 1993; Qian *et al.*, 1994; Jin *et al.*, 2002), and are generally considered as potential oil exploration targets in these basins. However, clastic carbonates that were sourced directly from the catchment bedrock have been rarely reported from these basins. Although there are numerous examples of lake basins with clastic carbonates that were largely controlled by the bedrock lithology of their drainage basins elsewhere (e.g. Szulc & Cwizewicz, 1989; Gierlowski-Kordesch, 1998; Blair, 1999a; Yuste *et al.*, 2004; Nichols & Thompson, 2005), they generally differ from the example reported here with regard to tectonic (i.e. subsidence) and climatic conditions.

An example of clastic carbonates deposited in a rapidly subsiding, sediment-starved deep lake rift basin of the Shulu Sag of Jizhong Depression, North China is presented here. The carbonate succession occurs in the base of basin fill both on the steep, fault-bounded, and relatively gentle, hinged slopes. The hinged slope was better constrained by seismic and borehole data, and is the focus of this study. The goal of this study is to unravel the depositional features, geometries, and evolution of these source-controlled carbonates in a rapidly subsiding, half-graben lake basin, on the basis of detailed core descriptions, well log analyses, and seismic facies and sequence analyses. This study will improve understanding of the relationship of clastic carbonate deposition to the provenance, tectonism and climate in the rift basin.

GEOLOGICAL SETTING AND STRATIGRAPHY

Tectonic setting

From the latest Cretaceous through Tertiary, transformation of regional stress regimes from sinistral transpressional to dextral transtensional faulting (NE- or NNE-trending), as well as crustal extension and thinning beneath the Bohai Bay area, North China, were induced by the collision between the Indian and Eurasian continental plates, i.e. the Himalayan Orogeny (e.g. Ye *et al.*, 1985; Zhang, 1985; Zhou *et al.*, 2004). This tectonic process created an overall NE–SW trending rhomb-shaped (pull-apart) basin infrastructure (with a series of grabens and half-grabens, e.g. the Jizhong Depression) bounded by the Yanshan, Luxi, Taihang and Jiaodong-Liaodong uplifts to the north, south, west and east, respectively (Fig. 1) (e.g. Hellinger *et al.*, 1985; Ye *et al.*, 1985; Zhang, 1985; Nábélek *et al.*, 1987; Nilsen & Sylvester, 1995; Zhou *et al.*, 2004).

The Shulu Sag is located in the south-western corner of the Jizhong Depression (Fig. 1), formed through downthrowing of the hangingwall of Xinhe dextral extensional fault trending NE–SW from the early Tertiary time in the context of a dextral transtensional tectonic regime in the Bohai Bay area. Within this half-graben, basin fills gradually onlapped updip upon the gentler western slope linking to the Ningjin uplift upslope (Figs 2 and 3). Other NE–SW trending faults, commonly normal faults in nature, were also active during the Tertiary within the basin (Figs 2B and 3). There is another set of nearly

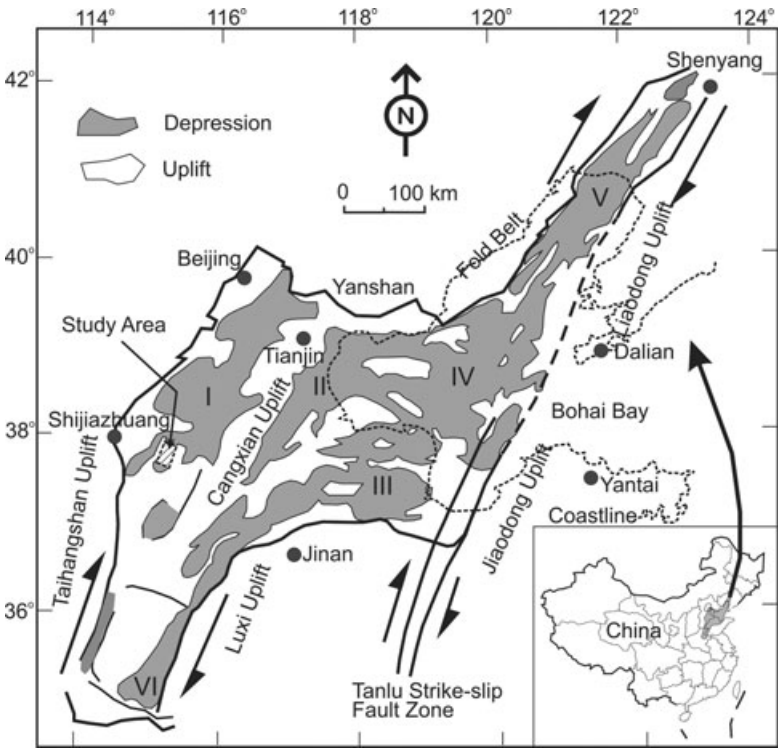

Fig. 1. Tectonic setting of the Shulu Sag half-graben during the Tertiary, located in the south-western corner of Jizhong (central Hebei) Depression (I) (synthesized from Ye *et al.*, 1985; Nábélek *et al.*, 1987; Zhou *et al.*, 2004). Other sub-basins in Bohai Bay of North China are Huanghua Depression (II), Jiyang Depression (III), Bozhong Depression (IV), Liaohe Depression (V) and Dongpu Depression (VI).

W–E to WNW–ESE trending faults, formed during the Middle Jurassic to Late Cretaceous Yanshanian Orogeny (e.g. Yang *et al.*, 2001), namely the Hengshui, Taijiazhuang and Jingqiu faults, in which the former one delimited the northern boundary of the Shulu Sag (Fig. 2B). These antecedent faults controlled the topographic relief within the basin, forming three segments: the northern, middle and southern segments (Fig. 2B). The middle segment is the focus of this study.

Stratigraphy

Bedrock stratigraphy

The basement of the Shulu Sag is the eastward-dipping, tilted block composed of double-layered Archean-Palaeoproterozoic metamorphic rocks and Meso-Neoproterozoic through Palaeozoic sedimentary strata. These units gradually subcrop westwards (Fig. 3A), so that the Cambro-Ordovician and Permo-Carboniferous strata are directly overlain by the Tertiary lacustrine basin fills (Figs 3 and 4). The Permo-Carboniferous strata, only localized in the basin centre, are mainly composed of marine coal-bearing siliciclastics intercalated with minor limestones (Ye, 1983). Mid-upper Cambrian to Middle Ordovician strata are dominated by carbonate successions deposited on carbonate ramp systems; the Mid-Lower Cambrian successions, however, are dominated by siliciclastics intercalated with minor carbonates (Ye, 1983; Jiang *et al.*, 1996; Meng *et al.*, 1997; Shi *et al.*, 1997).

Basin-filling stratigraphy

From the top to bottom, the basin-filling strata, locally up to 6500 m thick in the depocentre, comprise the Pingyuan, Minghuazhen, Guantao, Dongying and Shahejie formations (Fig. 3), in which the Shahejie Formation can be further divided into three members: no. 1 (Es1), no. 2 (Es2) and no. 3 (Es3). The Shahejie 3, generally 0–2200 m thick and the focus of this study, consists of three units: (1) the basal clastic carbonates; (2) the middle argillaceous limestone (or marlstones) intercalated with shales; and (3) the upper dark grey mudstones interbedded with fine-grained sandstones. The Shahejie 2, generally 0–400 m thick, consists of brown to purplish red mudstones interbedded with pale grey fine-grained sandstones; it is unconformably overlain by the Shahejie 1 (Fig. 3). The Shahejie 1, commonly 0–800 m thick, contains the basal white gypsum, gypsiferous mudstones and brown mudstones, which pass upwards into light grey fine-grained sandstones, siltstones and purplish red mudstones. The Dongying

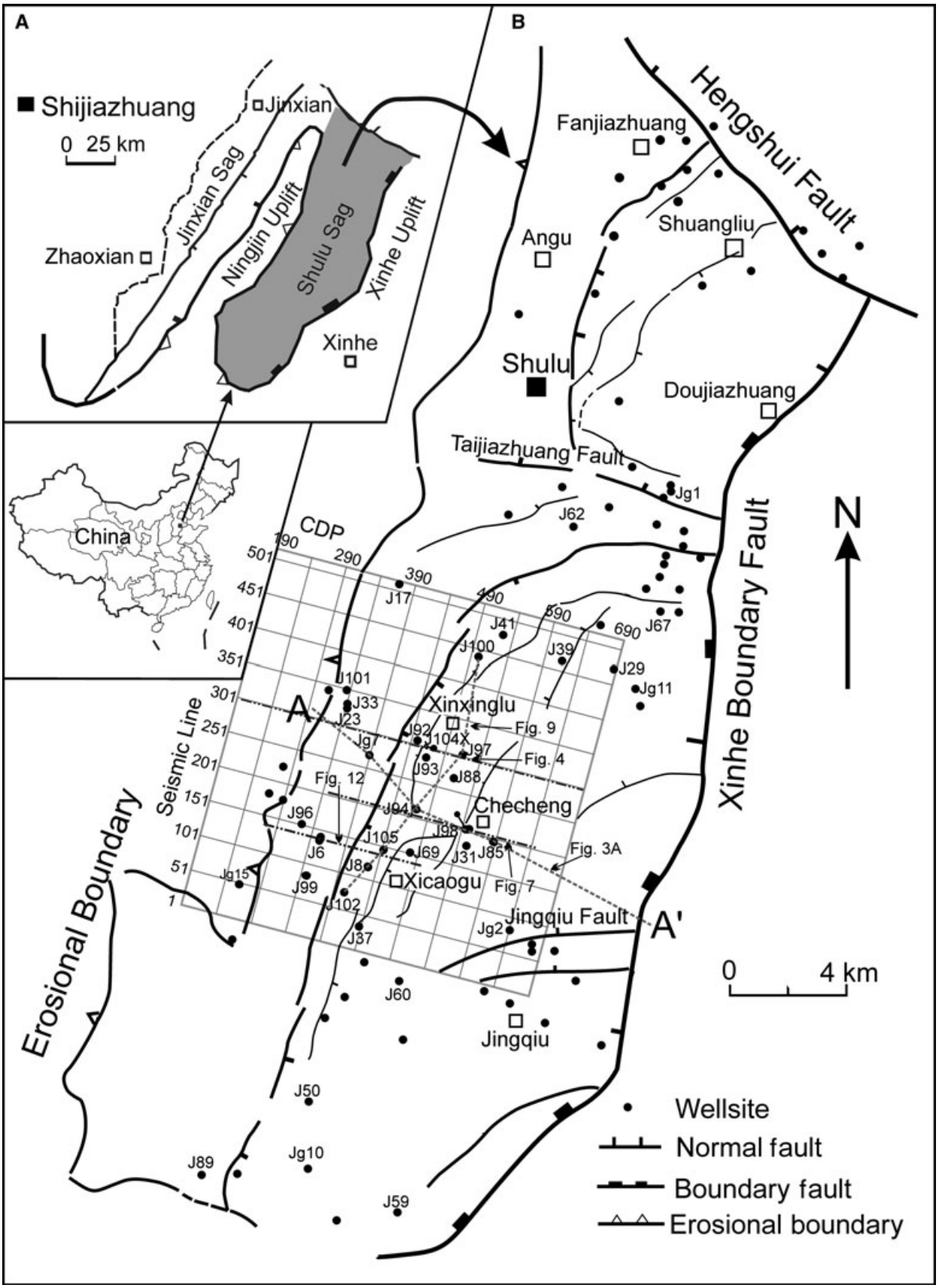

Fig. 2. (A) Sketch of Shulu Sag. (B) Structural map of Shulu half-graben. Three segments are delimited by the Taijiazhuang and Jingqiu faults. Section A–A′ is the location of Fig. 3A. Inset grid diamond is the seismic array.

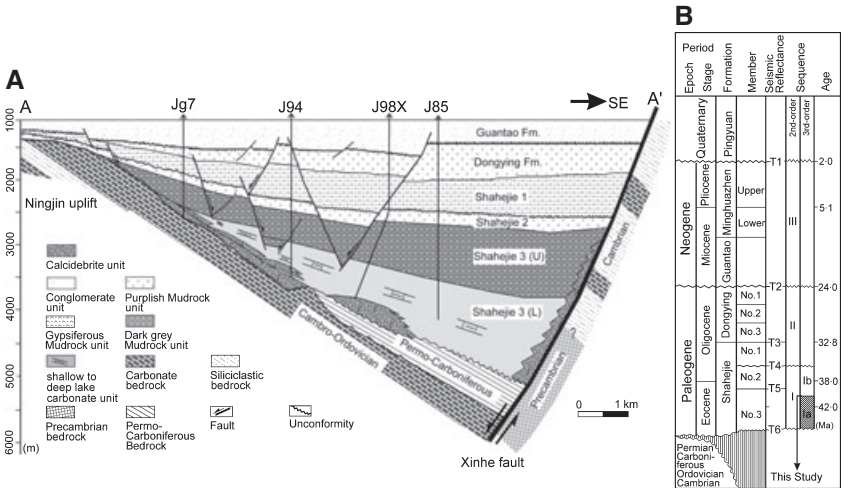

Fig. 3. (A) Transverse section (A–A′) across the middle segment of the Shulu Sag, exhibiting a typical half-graben geometry bounded by the Xinhe fault to the east, based on 3D seismic and borehole data (partly from Figs 7 and 8). Carbonate successions unconformably overlie the basement that consists of Cambro-Ordovician and Permo-Carboniferous strata below the hinged western slope, and Cambro-Precambrian rocks beneath the fault scarp to the east. See Fig. 2 for location. (B) Stratigraphic systems and sequence framework of the Shulu Sag. The age data are derived from Ye *et al.* (1993).

Formation is characterized by purplish red mudstones interbedded with pale grey siltstone/fine-grained sandstones, which are unconformably overlain by the Guantao Formation (Fig. 3). The Guantao Formation generally commences with variegated basal conglomerates, passing upwards into pale grey sandy conglomerates and sandstones interbedded with purplish red mudstones. The Minghuazhen Formation is characterized by unconsolidated sandy gravels interbedded with brownish red clays, which are unconformably overlain by the Quaternary Pingyuan Formation (Figs 3 and 4). The Pingyuan Formation commonly starts with alluvial (or pluvial) sands, grading upwards into yellow clayey silts and fine-grained sands.

RESEARCH METHODOLOGY

This study utilizes a comprehensive approach that integrates with seismic interpretation, wireline log analysis, and descriptions and petrographic studies of core samples and cutting fragments. Depositional sequences and systems tracts were identified mainly based on seismic

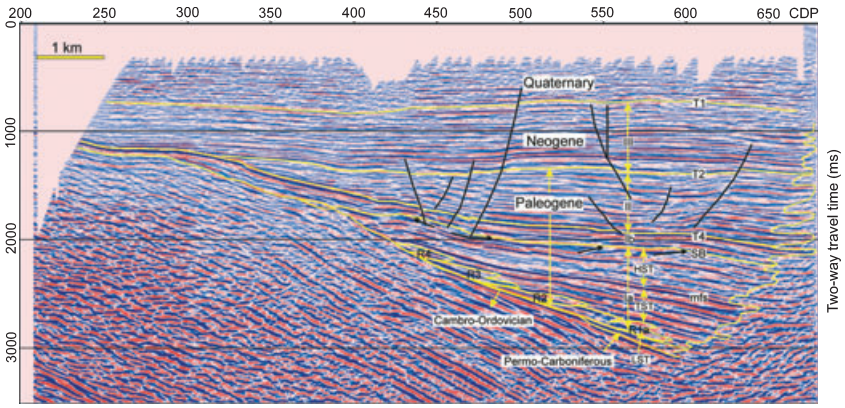

Fig. 4. Seismic line (line 300) across the entire basin, showing overall divergent reflection patterns and typical half-graben geometry of the Shulu Sag. Reflection terminations are highlighted by arrows. R1a–R4 are reflection patterns of carbonate rudstone packages. Note the mounded to lobate reflection patterns (R1a) near the bottom of the hinged ramp, very close to the border fault to the east. No valley-filling reflection is present on the mid-upper slope as shown in Figs 3 and 7. See Fig. 2 for location. T1, T2 and T4 are major seismic reflectances in the basin; I–III are second-order sequences (cf. Fig. 3B).

reflection patterns and terminations; these were further constrained by forward stratigraphic modelling (synthetic seismograms), which integrated seismic data with well logs and core data along key crossing-well seismic profiles. Stratigraphic-depositional cross-sections along and across the depositional dip were constructed to delineate the tempo-spatial distribution of the alluvial carbonate facies in the lake. Accordingly, a depositional model for the clastic carbonates and their equivalents in the Shulu Sag was then established.

FACIES ASSOCIATIONS OF THE CARBONATE UNIT

The carbonate unit occurs in the base of the basin-filling succession (i.e. the Shahejie 3 Member) during the early stage of basin filling (Fig. 3). In this study, nine major lithofacies are identified and differentiated on the basis of the size of carbonate particles (from rudstone to lutite) and their textures (Table 1), including the matrix-supported carbonate rudstones (LF1; Fig. 5A and B), clast-supported carbonate rudstones (LF2; Fig. 5C–E), pebbly carbonate arenites (LF3; Fig. 5F), carbonate arenites (LF4; Figs 5G,H and 6C), calcrete carbonates (LF5; Figs 5B and 6D), calcisiltite-calcilutites (LF6; Figs 5H,I,L and 6E,F,H), laminated calcilutites (LF7; Figs 5J and 6G), calcareous shales (LF8; Fig. 5K) and oil shales (LF9). The composition of lithoclasts covers a wide spectrum of carbonate lithologies, including limestones and dolostones (e.g. Figs 5A–E and 6A; Table 1), and rare siliciclastic quartzarenite/chert and mudstone (~1%). Rudite lithofacies are composed of either monomictic or polymictic lithoclasts of limestones and/or dolostones, and therefore will be designated with the 'carbonate' prefix. In the coarse lithofacies, marine fossil fragments are locally present within gravel- and sand-sized lithoclasts of limestone (e.g. Fig. 6B), whereas, they are absent in the matrix.

The above lithofacies can be grouped into five facies associations: mid-proximal alluvial fan, distal alluvial fan, fan fringe, moderately deep lake, and deep lake associations, in which the first two associations constitute a domain of alluvial fans dominated by carbonate rudstone packages. The lake facies domain, including the fan fringe, moderately deep and deep lake associations, are dominated by fine-grained, laminated carbonate-shale packages. The tempo-spatial distribution of these facies associations is illustrated in Figs 7–10.

Mid-proximal alluvial fan association

Description

This facies association mainly includes matrix-supported carbonate rudstones, clast-supported carbonate rudstones with minor pebbly carbonate arenites (or rare carbonate arenites) and rare calcrete carbonates (Table 1; Fig. 11). They occur in the basal rudstone unit perched on the mid-upper slope and at the bottom of the slope, and subsequent backstepped rudstone lobes (Figs 4 and 7–10).

In the basal rudstone unit on the mid-upper slope between seismic lines 50–290 and CDPs 280–490 (R1b, see Figs 7, 10A and 12), and the proximal portions of backstepped rudstone lobes (R2–R4) (i.e. in well J8; see Fig. 9), these carbonate rudstone units, generally 100–250 m thick, are dominated by thick- to massive-bedded, matrix-supported carbonate rudstones with rare basal scours (Figs 8 and 9), in which the carbonate lithoclasts are generally angular, disorganized, occurring as rafts within the matrix; they commonly pass upwards into clast-supported carbonate rudstones with lithoclasts accounting for 70–90% by volume, and locally into pebbly carbonate arenites (Figs 5A–C and 11A). No grading or reverse grading is present within stratified beds (Fig. 11A). Thin calcrete carbonates (i.e. laminar crusts), commonly eroded by overlying carbonate rudstones, are intercalated locally (Fig. 5B).

Downdip along the slope, in the basal rudstone facies at the bottom of the hinged slope (R1a) and central portions of backstepped rudstone lobes (R2–R4) (e.g. well J100, see Fig. 9), the whole rudstone successions are generally 50–150 m thick (Figs 8 and 9). In these localities, rudstone packages are dominated by thick-bedded (locally massive-bedded), clast-supported carbonate rudstones commonly with basal scours (Fig. 11B and C), in which carbonate lithoclasts are generally subangular to subrounded, with slightly smaller gravel particles and less fine-grained matrix (e.g. Fig. 5D and E), compared with the facies described above. Carbonate arenites (or pebbly carbonate arenites) and argillaceous calcisiltites are intercalated locally (Figs 8, 9 and 11C). Calcrete horizons (i.e. alveolar texture) are intercalated, particularly in the upper part of the basal carbonate rudstone lobes (i.e. at well J97) (see Figs 6D and 9). This facies association, along with the

Table 1. Summary of carbonate lithofacies in the base of the Shulu Sag, Jizhong (central Hebei) Depression

Lithofacies	Description	Wireline log response	Interpretation
Matrix-supported carbonate rudstone (LF1)	Grey to dark grey, generally 10s of centimetres to 10s of metres stratified beds. Monomictic to polymictic lithoclasts of carbonates, mainly including bioclastic mudstone/wackestone, dolostone, dolomudstone, microbialites, ooidal (or peloidal) grainstone, edgewise conglomerates, with rare siliciclastic quartzarenite/chert and mudstone. Angular to subangular clasts common, 1–20 cm, rarely up to 80 m in size. Disorganized and matrix-supported textures with abundant matrices ranging from calcilutite to granules with variable clay contents. Structureless (massive) with rare scoured bases. No grading (or reverse grading) common. Fossil fragments (trilobites, crinoids/echinoids, brachiopods, bryozoans and ostracods) within carbonate lithoclasts locally. Calcrete carbonates intercalated locally. Gradation to LF2 locally.	Low to intermediate amplitudes of spontaneous (Sp) and resisitivity (Rs) curves, generally serrated, gradual upper and lower contacts common	Subaerial debrisflow (or mud flow) deposits in mid-proximal alluvial fans
Clast-supported carbonate rudstone (LF2)	Grey to light grey, 10s of centimetres to 10s of metres thick stratified beds. Similar clast compositions as those in LF1. Subangular to subrounded lithoclasts common, several mm to 20 cm in size. Clast-supported textures commonly, matrix-supported textures locally. Stratified beds with basal scours common, no grading (or reverse grading) common. Similar fossil fragments within lithoclasts as in LF1. Gradation from LF1 locally	Intermediate to high amplitudes of Sp and Rs curves, variable shapes of combined curves (cylinder, bell and funnel), gradual upper and lower contacts common	Debrisflow deposits in mid-distal fans, might have been reworked by flow water or longshore currents
Pebbly carbonate arenite (LF3)	Grey to dark grey, 10s of centimetres up to several metres thick. Diversified composition of carbonate lithoclasts as those in LF1 and LF2. Subangular pebble lithoclasts as rafts in the carbonate arenites (or calcisiltites), no grading or reverse grading bedding. Locally similar fossil fauna as those in the facies described above. Calcilutite (or laminated calcilutites) intercalated common	Intermediate to intermediate high amplitudes of Sp and Rs curves, generally serrated	Sandy debrisflow deposits in sublacustrine setting
Carbonate arenite (LF4)	Grey to dark grey, a few centimetres up to 1 m thick. Diversified carbonate sands of lithologies. Rare granule- and pebble-sized carbonate lithoclasts as rafts. Subangular to subrounded sand-sized lithoclasts. Matrix-supported textures common. Locally Similar fossil fragments with clasts as those above. Intercalated in calcilutites (or laminated calcilutites) and calcareous shales commonly, in rudstones locally	Generally intermediate amplitudes of Sp and Rs curves, not well developed	Turbidity deposits in sublacustrine setting; might have been reworked in distal fan by lake waves/ currents
Calcrete carbonate (LF5)	Buff-coloured, generally <10 cm thick. Laminar crust and alveolar/tubular texture common, rare rhizoconcretion. Intercalated in basal carbonate rudstone unit	Too thin to have a specific response	Subaerial exposure under an intermediate climatic condition

Table 1. Continued

Lithofacies	Description	Wireline log response	Interpretation
Calcisiltite-calcilutite (LF6)	Dark-coloured, several centimetres up to 10 m thick. Visible silt- to mud-sized clastic carbonate and terrigenous grains, dominated by carbonate minerals (calcite: 59–86%, dolomite: 1–18%) with subordinate clay (5–17%) and detrital minerals (4–10%) (Table 2); containing organic matter (0.5–2.5%) and pyrite, and rare authigenic glauconite, particularly in calcilutite. No lamination to thick lamination (3–10 mm). Bioturbation locally. Rare ostracod shells, fish remains and plant fragments	Low to intermediate amplitudes of Sp and Rs, smooth to serrated curves	Moderately deep to deep lake deposits by dilute density underflows, under a semi-humid to a humid climate
Laminated calcilutite (LF7)	Dark-coloured, several centimetres to a few metres thick. Carbonate minerals (calcite: 52–73%, dolomite: 5–22%) dominant with subordinate clay (5–24%) and detrital minerals (4–14%) (Table 2); relatively high organic matter and pyrite in bulk sample as in LF6. Extensive varve-like lamination (<3 mm thick) indicated by alternating dark-coloured, argillaceous-rich and light-coloured, carbonate-rich laminae, relatively high content of pyrite, glauconite, organic matter and clastic particles in dark layers. Rare bioturbation. Rare ostracod shells, fish remains and plant leaves	Low amplitudes of Sp and Rs, smooth to serrated curves	Anoxic, stratified deep lake, under a semi-humid to a humid climate
Calcareous shale (LF8)	Dark-coloured, several centimetres up to a few metres thick. Increased clay and detrital minerals (>50%) when compared with LF7 (Table 2). Extensive varve-like laminations (<3 mm thick) as in LF7, relatively high content of pyrite, glauconite, organic matter and clastic particles in dark layer as well. Slump folds locally, rare bioturbation. Rare ostracod shells, fish and plant remains	Lowest to low amplitudes of Sp and Rs, smooth to serrated curves	Anoxic, stratified deep lake, with increased terrigenous suspension fluxes, under a semi-humid to a humid climate
Oil shale (LF9)	Brownish grey to dark grey, several centimetres to ~5 m thick. Higher organic matter (generally with TOC of 2.5–12.5%). Very thin lamination (0.1–0.3 mm thick common). Intercalated in LF7 and LF8 commonly.	Low amplitudes of SP, high amplitudes of Rs	Anoxic, stratified deep lake, with a high bioproductivity, under a more humid climate

distal fan association described below, forms the main framework of fan-shaped rudstone bodies at the edge of lake (Fig. 10).

Interpretation

The angularity of clasts and the restriction of the carbonate rudstones along the basin margin indicate a relatively short distance of transport. The matrix-supported rudstones with angular, disorganized and poorly sorted lithoclasts (e.g. Fig. 5A and B) suggest that they were deposited by cohesive debrisflows (or mud flows) (Lowe, 1982; Mulder & Alexander, 2001); the poor-sorted gravels and abundant silt- and mud-sized particles could have greatly promoted the transformation of water-saturated sediments on steep slopes into a debrisflow through entrainment of air and water (i.e. flashy rainfall and/or groundwater discharge), and increased pore pressures and decreased shear strengths of sediments (Hampton, 1972; Blair, 1999a,b) during transport down steep slopes. The clast-supported rudstones with angular to subangular, poorly sorted lithoclasts, and a variable, but sometimes small (10–30%), proportion of muddy material (Fig. 5C) are also interpreted as having been deposited by debrisflows (e.g. Lowe, 1982; Mulder & Alexander, 2001), due to increased pore pressures and surface tension by adding water and gravel-sized particles during the movement under subaerial settings (Major & Iversion, 1999; see documentation below). Thus the reverse grading and gradation from matrix- to clast-supported rudstones in some horizons suggests increased entrainment of gravel-sized particles during the course of downslope movement of debrisflows. The thin intercalations of carbonate arenites or pebbly arenites (e.g. Fig. 11) are considered to be deposits of highly concentrated flows (Mulder & Alexander, 2001) or deposits from sandy debrisflows (Shanmugan, 1996) transformed after the original debrisflow initiation. The basinward-increasing abundance of stratified rudstones may reflect increased influences of episodic ephemeral flooding processes (Miall, 1978; Abdul Aziz *et al.*, 2003). The fan-shaped to arcuate geometry of rudstone bodies in planar view, constrained by numerous seismic profiles (e.g. Figs 4, 7 and 10), suggest that they were formed in alluvial fan environments along the lake edge. The basal rudstone units on the mid-upper slope, however, are considered as perched alluvial fans because they filled the palaeovalleys by axially extending along the depositional strike, rather than downslope-extending along depositional dip (Figs 7, 10 and 12). In this case, those debrisflows that moved through the palaeovalleys on the mid-upper slope could have been partially retained on the mid-upper slope, forming perched alluvial fans; the sediments would move further downslope to the bottom of the slope to form basinal or lake-margin alluvial fans.

The presence of thin calcrete horizons (Figs 5B, 6D and 11A), particularly in the basal rudstone unit on the mid-upper slope and the proximal part of rudstone lobes at the bottom of the slope, suggests that these rudstone units, at least, temporarily were formed subaerially (Esteban & Klappa, 1983; Tucker & Wright, 1990). The alveolar septal and tubular fabrics (Fig. 6D) in calcrete horizons show evidence of apparent biological activity around root systems during pedogenic processes (Tucker & Wright, 1990), commonly occurring under intermediate climatic conditions (Platt & Wright, 1992). This climatic scenario is further supported by the absence of evaporites in these rudstone packages. Therefore, the basal carbonate rudstone units in the basin fill on the hinged western slope of Shulu Sag were mostly deposited in subaerial alluvial systems under an intermediate climatic regime.

Distal alluvial fan association

Description

This facies association is characterized by clast-supported carbonate rudstones, intercalated with pebbly carbonate arenites, calcisiltite-calcilutites, locally with laminated calcilutites and calcareous shales (Table 1; Figs 8, 9 and 11B). It occurs in the distal part of the rudstone fans, and interfingers with the lake facies association basinwards.

The clast-supported carbonate rudstones are relatively thin, from 10 to 15 m thick, in which carbonate lithoclasts are generally subangular to subrounded in shape (Fig. 5D). No grading to weak normal grading occurs in individual stratified beds. Locally, these rudstones pass upwards into thin-bedded pebbly carbonate arenites and/or carbonate arenites (generally <1·5 m thick) (Fig. 11B), which are either structureless or reversely graded (Fig. 5F). Rafted pebbles are locally present in arenites (Fig. 5H). Fine-grained limestone intercalations include calcisiltite-calcilutites, laminated (or varved) calcilutites and calcareous shales; they are generally <2 m thick and commonly contain argillaceous and detrital materials in composition (Table 2). Thin laminations (varve-like) are extensive in the latter two

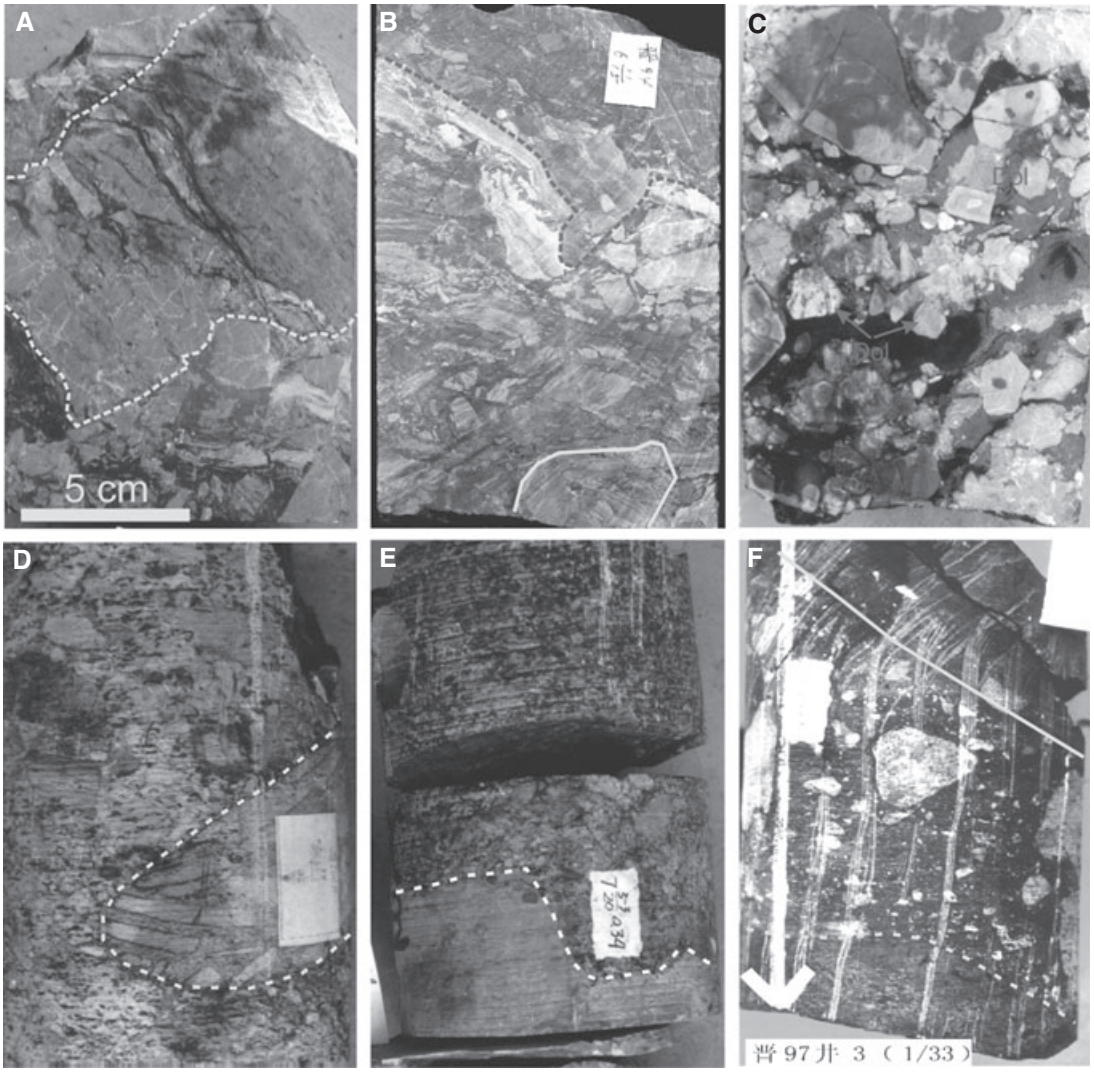

Fig. 5. Core photos showing different types of carbonate lithology. (A) Matrix- to clast-supported carbonate rudstones with angular and poorly sorted lithoclasts. Note the angular cobble-sized lithoclast (within the dashed line) of original lithology of dololaminite. The clasts were highly fractured during burial. From well J94, at 3543·1 m. (B) Matrix-supported carbonate rudstone with angular lithoclasts floating in the matrix. Note the buff-coloured laminated limestones (dashed arrows), probably the laminar calcretes, which were eroded during the deposition of the overlying rudstones (dashed line). From well J94, at 3545·65 m. (C) Angular to subangular, matrix- to clast-supported carbonates composed of clasts of different carbonate lithologies, showing vague reverse grading. Matrix consists of variable-sized clastic carbonates from calcilutites to granule-sized particles. Note the light-coloured dolomite lithoclasts (Dol). From well J94, at 3335·7 m. (D) Subangular to subrounded, clast-supported carbonate rudstone. Note the cobble-sized lithoclasts, originally composed of edgewise conglomerates (within the dashed line). From well J100, at 3229·8 m. (E) Pebble-sized, clast-supported carbonate rudstone, and the underlying weakly laminated calcilutite. Erosional contact delineated by the dashed line. From well J98, at 4007 m. (F) Pebbly carbonate arenites showing reverse grading, with erosional contact with the underlying carbonate arenites (dotted line) and capped by laminated calciluites (solid line). Arrow points to the bottom. Vertical strips are scratches caused by drilling. From well 97, at 3637·4 m. (G) Massive coarse-grained carbonate arenites. From well J97, at 3867·6 m. (H) Carbonate arenites intercalated with argillaceous calcisiltites (dotted lines highlight contacts). Note the carbonate lithoclast rafts (hollow arrows) in the upper part of arenites. White calcite-filling veins are postdepositional. Arrow points to the bottom. From well J97, at 3456·5 m. (I) Light-coloured calcisiltites with thick (3–10 mm) lamination capped by dark coloured calcilutites. Arrow points to the bottom. From well J94, at 3114·4 m. (J) Laminated calcilutite displaying millimetre-scale, varve-like laminae of alternating light-coloured carbonate-rich and dark argillaceous-rich couplets. Note the vertical scratches caused by drilling. From well J94, at 3152 m. (K) Well-laminated calcareous shale with varve-like lamination and slump folds. Note the oil-stained fractures. From well J97, at 3452 m. (L) Mottled laminated calcilutite, with oil-stained fractures. From well J100, at 3228 m. See Fig. 2 for locations of all wells. Refer to Figs 7 and 8 for the depositional context.

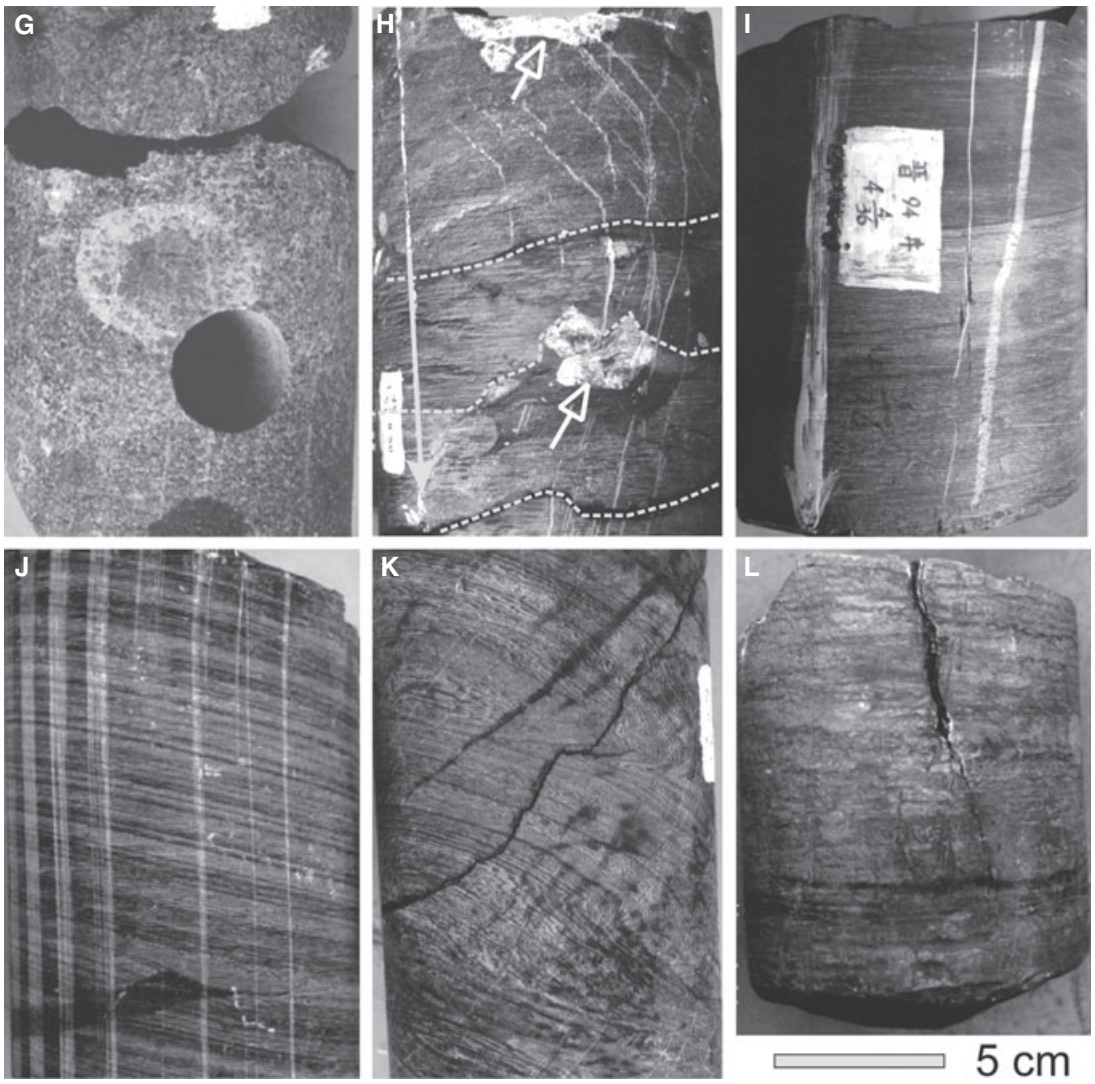

Fig. 5. Continued

fine-grained lithologies (Fig. 5J and K; Table 1). Laminations are represented by alternating light grey carbonate-rich and dark grey argillaceous-rich, and clastic-rich laminae; the dark laminae usually are slightly coarse with silt-sized clastic carbonate and siliciclastic grains, and contain abundant pyrite (Fig. 6G). Slump folds (Fig. 5K) and bioturbations (Figs 5L and 6H) occur locally. Rare glauconite and minor biotic fragments (ostracod shells, fish remains and plant leaves) occur within these fine-grained limestones (Figs 6F and 11), particularly well constrained in the basinal equivalents of the backstepped rudstone lobes.

Interpretation

The clast-supported carbonate rudstones, as documented above, are interpreted as having been mainly formed by debrisflows. The increased roundness and decreased thickness of rudstone successions point to an increased transport distance of sediment loads and/or wave/current reworking along the shoreline; preferred orientation of distal rudstone lobes along the shoreline (Fig. 10) was probably a response to redistribution by current reworking. Pebbly carbonate arenites are interpreted as having been deposited by concentrated (or high) density underflows or sandy debris underflows within the sublacustrine setting, based on their occurrences and structures (structureless or reverse grading). Thin-bedded carbonate arenites were probably deposited from turbidity currents, and calcisiltites from low-density turbidity currents as a result of progressive entrainment of water and sediment dilution. They may be the distal sub-

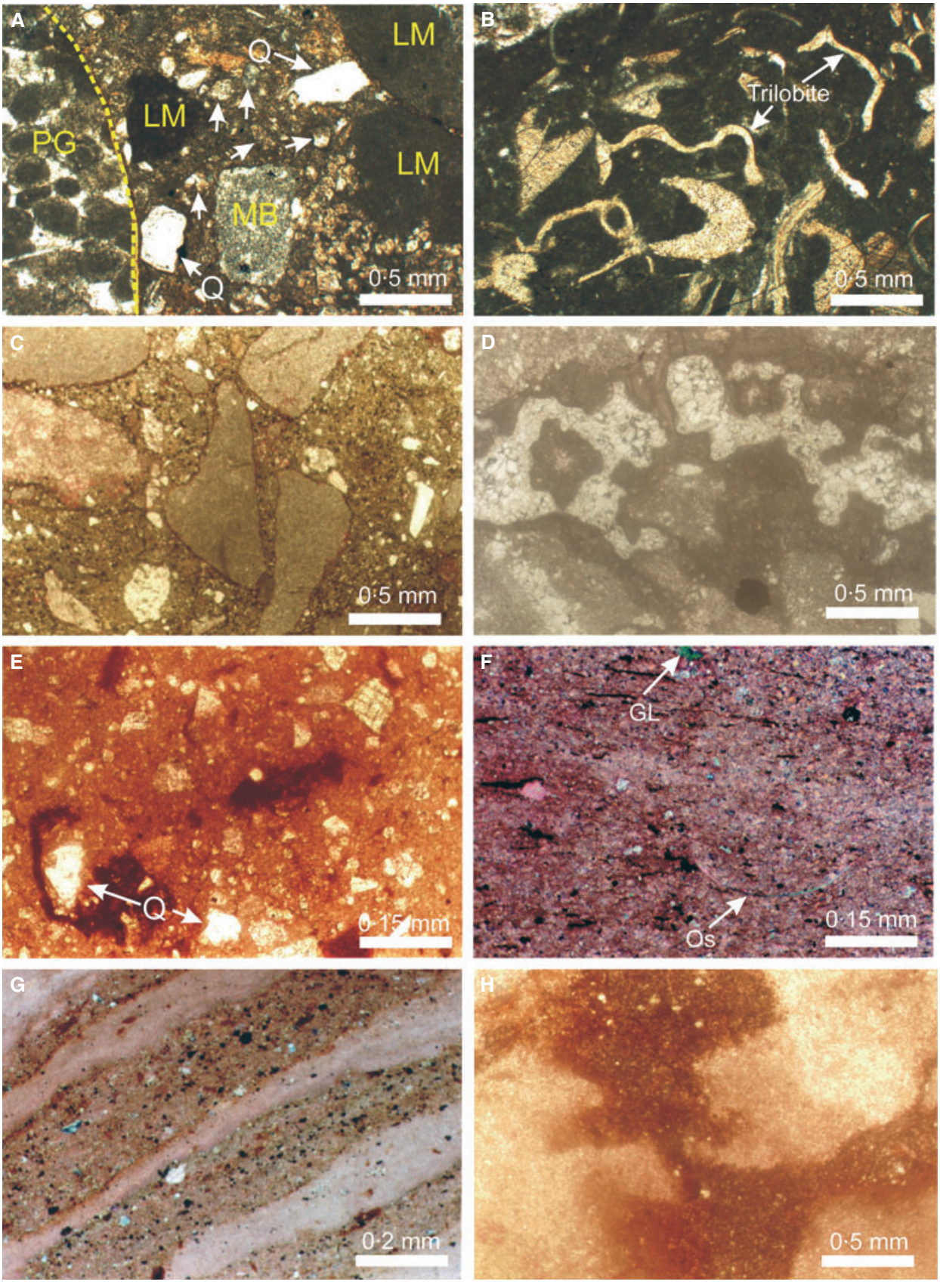
A
LM
Q
LM
PG
LM
MB
Q
0·5 mm
B
Trilobite
0·5 mm
C
0·5 mm
D
0·5 mm
E
Q
0·15 mm
F
GL
Os
0·15 mm
G
0·2 mm
H
0·5 mm

Fig. 6. Photomicrographs of main carbonate facies. (A) Matrix-supported carbonate rudstone composed of variable lithoclasts of ancestral carbonate lithologies, i.e. peloidal grainstone (PG) and lime mudstone (LM). Matrix composed of carbonate clasts of ancestral lime mudstone (LM), microbialite (MR) and dolomite (arrows), and siliciclastic particles [i.e. quartz (Q) and argillaceous material]. Planar-polarized light. From well J97, at 3866 m. (B) A carbonate clast composed of ancestral bioclastic wackestone with typical Cambro-Ordovician marine fossil fragments, mostly echinoids, trilobites and ostracods. Planar-polarized light. From well J97, at 3866 m. (C) Matrix-supported carbonate arenites composed mainly of clastic carbonate particles of antecedent dolomudstone with rare siliciclastic grains (i.e. quartz). Matrix is mostly clastic calcisiltitic to calcilutitic grains, and siliciclastic muds. Planar-polarized. From well J97, at 3865·65 m. (D) Alveolar texture displaying contorted tubular cavities filled with subhedral to euhedral spar calcite, and interconnected walls of micrite (dark colour). Matrix is clastic dolomudstone. From well J97, at 3863·15 m. (E) Calcisiltite with irregular silt-grained dolomite grains of clastic origin and minor quartz grains (Q) and argillaceous content. Planar-polarized light. From well J97, at 3588·2 m. (F) Calcilutite showing weak lamination. Rare thin-shelled (planktonic?) ostracod shells (Os) and authigenic glauconite (GL) occur. Note abundant silt-sized carbonate particles of clastic origin and organic matter (black). Crossed-nichols. From well J104, at 3340 m. (G) Laminated calcilutite, displayed by alternating argillaceous-rich and carbonate-rich (micrite) lamina couplets. Pyrite and silt-sized calcareous particles also concentrate in the argillaceous-rich laminae. Planar-polarized light. From well J97, at 3452 m. (H) Bioturbated calcilutite showing a mottled appearance. From well J97, at 3449·77 m.

aqueous part of subaerial debrisflows discharged from the alluvial fans as a result of catastrophic flooding and landslides.

Intercalations of well-laminated calcilutites and calcareous shales (Fig. 5J and K) point to an occasional incursion of a thermally stratified, anoxic lake water over fan bodies in response to seasonal climate fluctuations and changes of detrital influx. Fine-grained sediments carried by overflows and interflows settled down to the anoxic bottom water during summer thermal stratification phase, forming the dark-grey slightly coarser-grained, pyrite-rich layer of a varve couplet. The remaining suspended and dissolved carbonate loads at the thermocline zone would have settled out (or precipitated) to form the carbonate-rich (micrite) layers during the breakdown of thermocline (unstratified phase) (cf. Sturn & Matter, 1978). Although glauconite is generally considered as being of marine origin (Odin & Matter, 1981), it does occur in lake deposits. For example, in the modern freshwater Fuxian deep graben lake (~155 m deep in maximum), Yunnan, Southwestern China, glauconite occurs at water

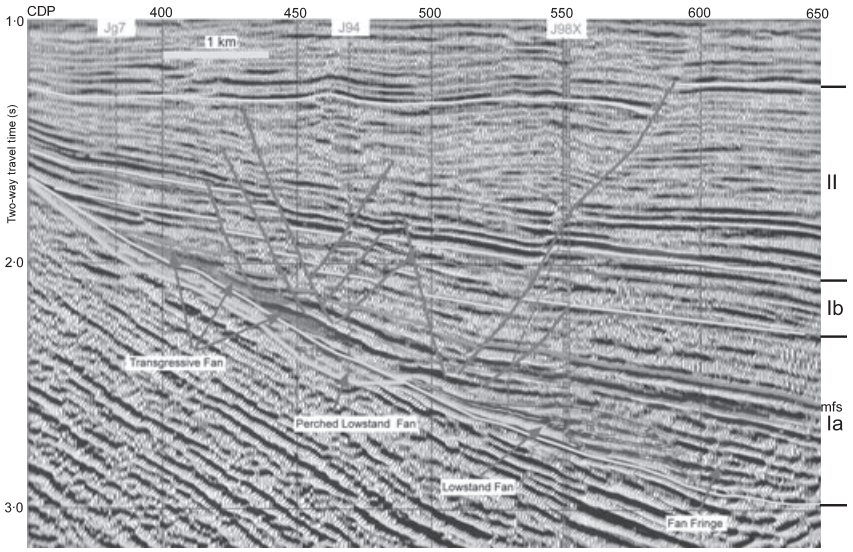

Fig. 7. Seismic line (line 203) across well J98X, roughly normal to the strike of basin (see Fig. 2 for location), showing the depositional sequences of early basin fill (Ia, Ib and II). Carbonate unit occurs in the mid-lower part of sequence Ia, above which is siliciclastic lacustrine deposits. Valley-filling reflections (perched fans, R1b) on the mid-upper slope and mounded reflection patterns (alluvial fans, R1a) on the lower slope are considered as lowstand deposits; backstepped hummocky reflections (R2–R4) upon the valley fills are transgressive deposits (see Fig. 8 for lithological information). Wells Jg7 and J94 are projected to this section along strike.

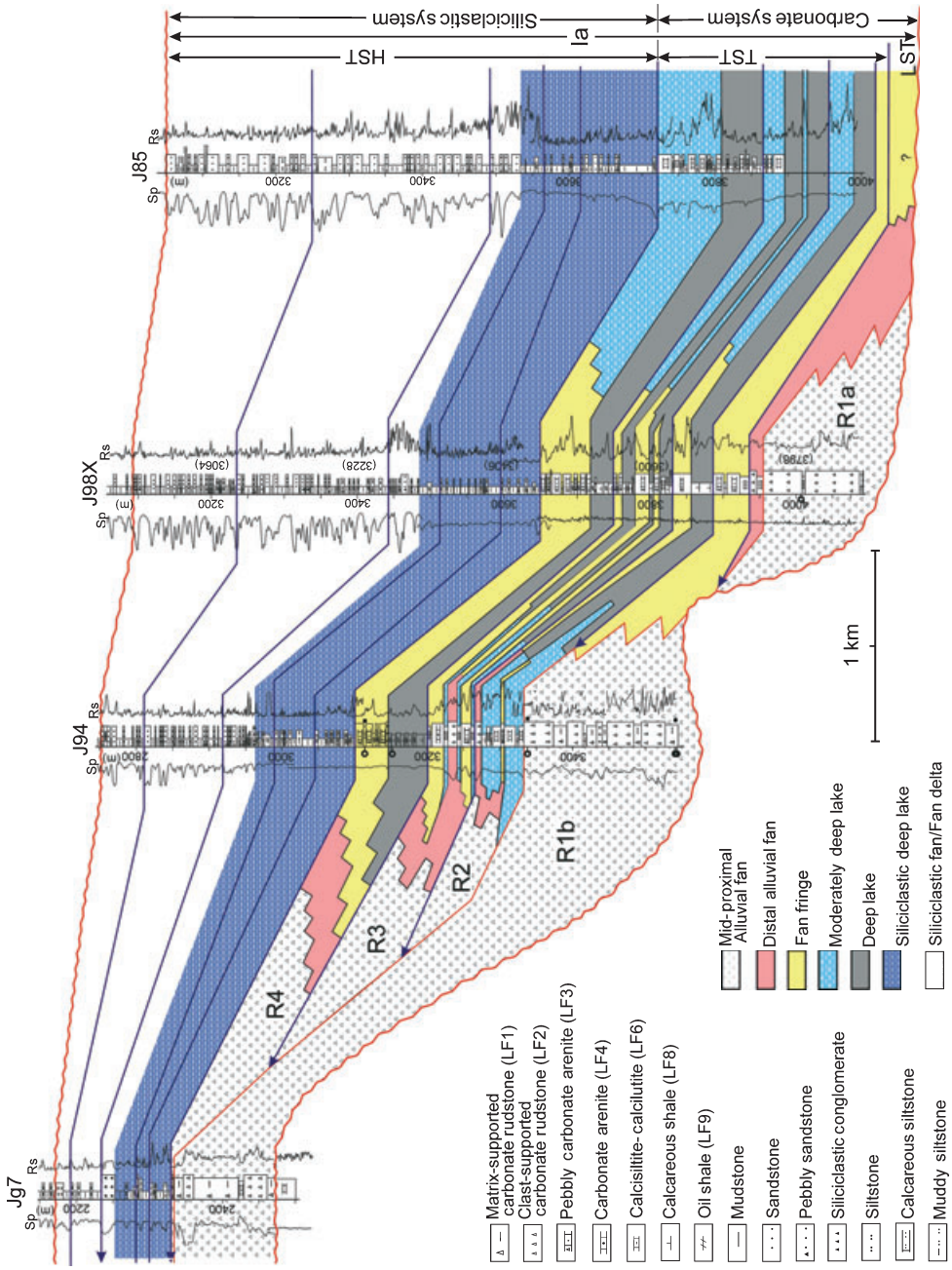

Fig. 8. Correlation of depositional facies and stratigraphic framework along depositional dip on the western slope (wells Jg7–J94–J98X–J85). Carbonate rudstone units occur both as lowstand (LST) (R1a–b) and transgressive (TST) (R2–R4) deposits of sequence Ia. The highstand (HST) deposits are composed exclusively of lacustrine siliciclastics. Well 98X has corrected vertical depths; these data are shown as bracket numbers opposite the well depth. Blue lines mark the boundary of parasequence sets, and those with arrows correspond to apparent high-amplitude reflectances in the seismic profile (see Fig. 7). Lithologies are interpreted mainly from well logs and cutting fragments. Circular markers on the left of litho-logs of well J94 are locations of petrographic data presented in Figs 5 and 6, those on the right (solid squares) are core intervals shown in Fig. 11A. See Figs 3 and 7 for a comparison of the depositional framework and facies distribution, and Fig. 2 for location.

depths of 35–150 m, on the relatively stable substrate with a low depositional rate, a suboxic to anoxic (Eh = 100 to −50 mv) and moderately alkaline lake bottom water (pH = 7–9) (Wang, 1983; Zhu *et al.*, 1989), similar to its marine counterpart (Odin & Matter, 1981). Accordingly, the presence of glauconite in the fine-grained limestones indicates a deep lake condition,

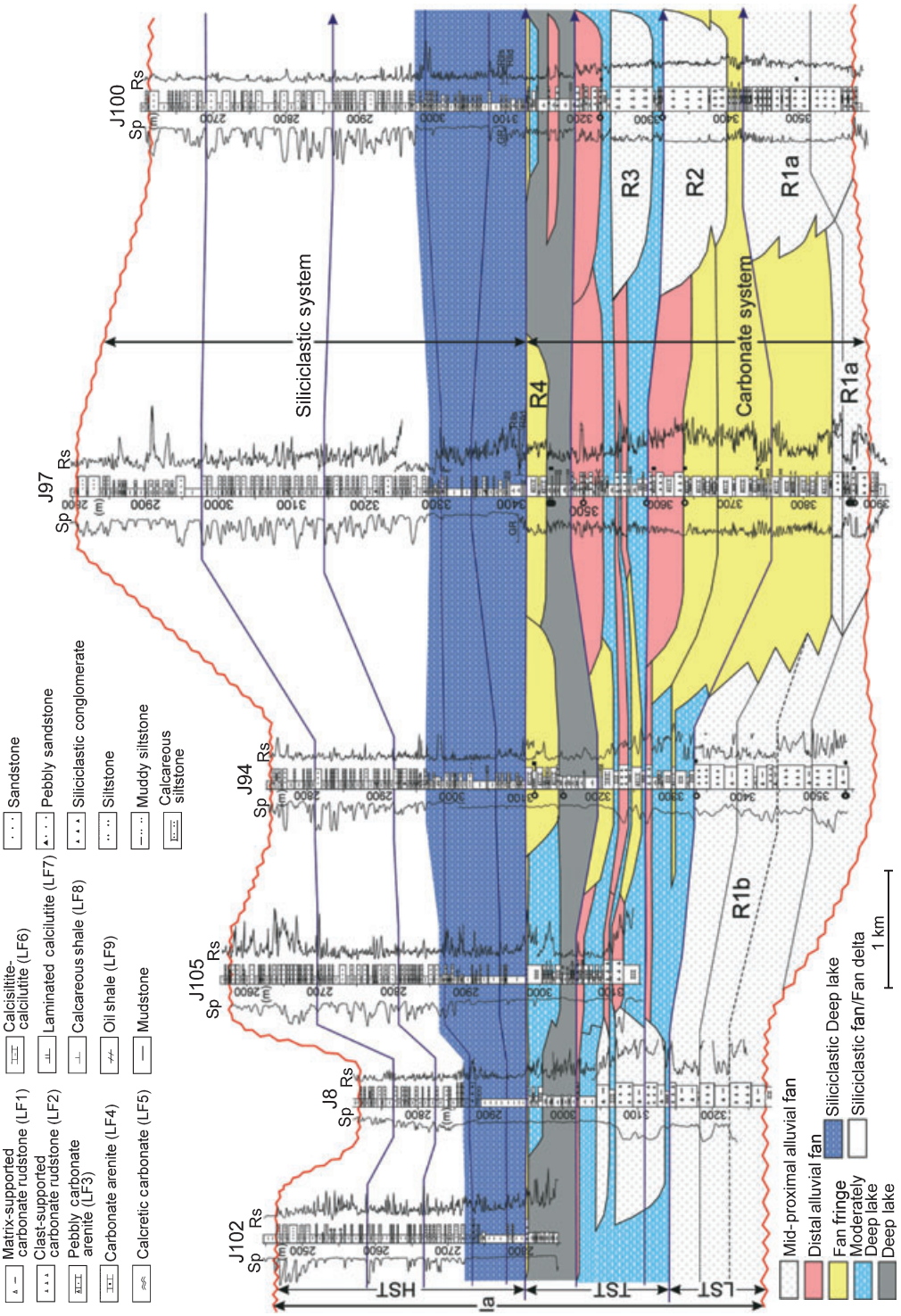

Fig. 9. Correlation of depositional facies and stratigraphic framework along the strike using wells J102–J8–J105–J94–J97–J100. Carbonate unit occurs in the LST and TST deposits (R1–R4 are rudstone units); HST deposits are exclusively lacustrine siliciclastics. Blue lines mark the boundary of parasequence sets, and those with arrows correspond to apparent high-amplitude reflectances in seismic profiles. Lithologies are interpreted mainly from well logs and cutting fragments. Circular markers on the left of litho-logs of wells J94, J97 and J100 are locations of petrographic data presented in Figs 5 and 6, those on the right (solid squares) are core intervals shown in Fig. 11. See Fig. 2 for location of the strike section.

probably with a connection to some extent with the open sea (Wei & Xu, 1993, see later discussion). A similar case history was reported from the Permian deep lake deposits in Junggar Basin, Western China (Zhao & Tang, 2000). The skeletal fossils (i.e. thin-shelled ostracods) in the fine-grained limestones (Fig. 6F) also support a deep lake condition. The presence of plant leaves in the fine-grained limestones suggests a semi-humid to humid climatic condition (Bohacs *et al.*, 2003), under which abundant precipitates would favour the formation of a deep lake regime (da Silva *et al.*, 2000). The presence of slump folds in fine-grained sediments reflects occasional instability of soft sediment substrate due to sediment overloading and/or other factors (i.e. earthquake shock, drop in lake level). Disturbance of varved layers reflects a transient oxygenation of bottom waters during deposition. Therefore, the intercalation of rudstones with fined-grained, well-laminated lake carbonates indicates interfingering of sublacustrine alluvial fans with a meromitic lake environment, pointing to a distal fan environment.

Fan fringe association

Description

This facies association is characterized by pebbly carbonate arenites (Fig. 5F) and carbonate arenites (Fig. 5G and H), locally with thin carbonate rudstones, which are intercalated either with calcisiltite-calcilutites, or with laminated calcilutites, calcareous shales and oil shales (Figs 7, 8 and 11C; Table 1). Pebbly carbonate arenites are generally 10s of centimetres to several metres thick, locally up to 10s of metres thick, in which pebble-sized lithoclasts occur as floating rafts in the matrix of carbonate arenites (locally calcisiltites); they are generally structureless or reversely graded and are vertically capped by fine-grained limestones similar to those listed above (e.g. Fig. 5F), or by oil shales. Carbonate arenites and rudstones, as described above, however, are of minor significance with respect to pebbly carbonate arenites. Oil shales, generally <5 m thick, are light brown to dark grey in colour and thinly laminated (submillimetre- to millimetre-scale). More rounded authigenic glauconite, slightly increased pyrite amounts and the same biota occur in the fine-grained limestones. This facies association commonly occurs in the upper part of upward-coarsening successions deposited on the mid-upper slope (Figs 7 and 8).

Interpretation

The dominance of pebbly carbonate rudstones and intercalations with fine-grained limestones similar to those described above and oil shales suggest a decreased influence of alluvial fans and an enhanced influence of a lake regime. The pebbly carbonate arenites (or carbonate arenites) with no grading or reverse grading suggest that they were deposited by the sandy debrisflows (or high-density to turbidity currents), which were developed from the debrisflows as a result of progressive entrainment of water and dilution during the course of downward transport (Hampton, 1972; Lowe, 1982; Fisher, 1983; Weirich, 1988; Mulder & Alexander, 2001). Intercalations of well-laminated calcilutites and calcareous shales indicate incursions of a short-lived thermally stratified, anoxic lake water mass. More rounded glauconite minerals and slightly increased pyrite amounts in the fine-grained limestones imply a more prolonged, non-disturbed substrate and more oxygen-deficient water bodies (Odin & Matter, 1981) during their formation, reconciling a deepened lake water column. In the absence of evaporative deposits, the occurrence of oil shales suggests a more quiescent, anoxic and stratified lake water column with no apparent agitation of density undercurrents, which was favourable for the prolonged accumulation of organic matter (see Talbot, 1988; Huc *et al.*, 1990). All of these features suggest that this facies association was deposited in the fan fringe with frequent gravity flows discharged from updip alluvial fans.

Moderately deep lake association

Description

This facies is characterized by calcisiltite-calcilutites intercalated with laminated calcilutites, calcareous shales and oil shales (Figs 8, 9 and 11). Calcisiltite-calcilutites, generally <10 m thick, are grey to dark grey and non-laminated to thickly laminated (0·3–1 cm thick, Fig. 5H and I) with bioturbations locally (Figs 5L and 6H). The rest, fine-grained lithologies, are generally dark-coloured and thinly laminated (varves, <3 mm) as described above. Generally the same authigenic minerals (pyrite and glauconite) and biota occur as in the previous facies association. This facies association commonly occurs in the middle part of an overall upward-coarsening succession deposited on the mid-lower slope (Figs 8 and 9).

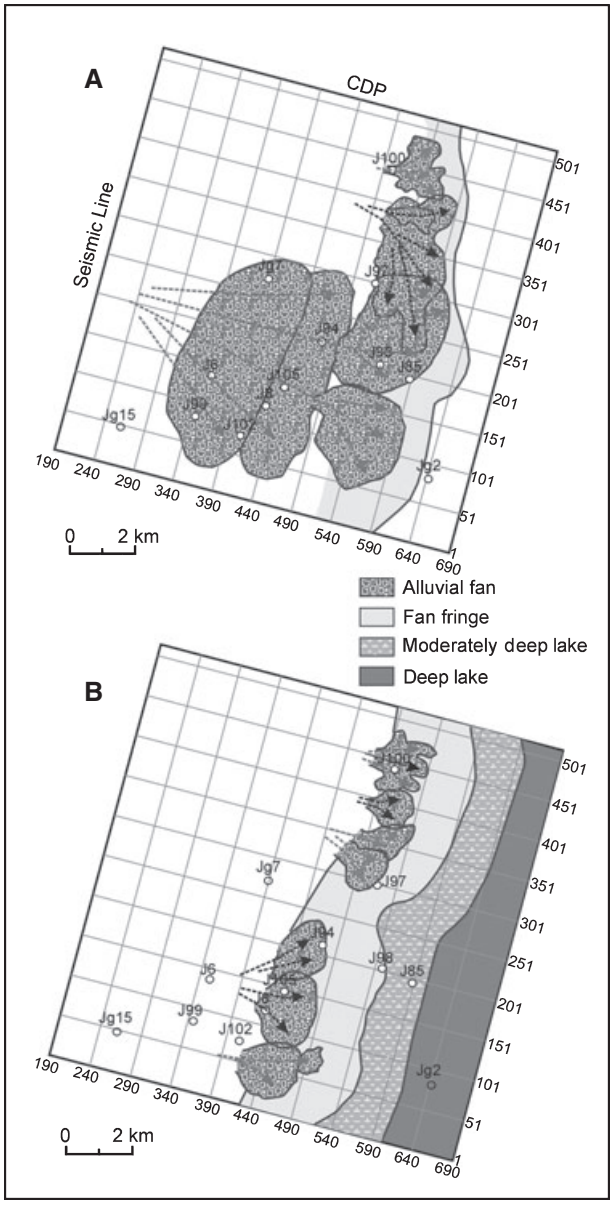

Fig. 10. Spatial distribution and evolution of carbonate alluvial fan/lake systems in sequence Ia, constrained by 3D seismic data and well logs. (A) Lowstand stage carbonate alluvial fan distribution in the middle segment of the Shulu Sag. Note the two NE–SW trending alluvial fan bodies perched on the mid-upper slope and the narrow shallow lake zone in the basin centre. (B) Carbonate alluvial fans during the early lake transgressive stage, which apparently became smaller and stepped updip with a largely expanded lake regime relative to panel A. Arrows represent possible flow directions on alluvial fans.

Interpretation

The dominance of calcisiltite-calcilutites, formed mainly by low-density (or dilute) turbidity underflows or the tail of turbidity currents (e.g. Hampton, 1972; Mulder & Alexander, 2001), points to a significantly decreased influence of alluvial fans away from the source area. On the contrary, the lake influence was greatly enhanced, as indicated by widespread dark-coloured, well-laminated calcilutites, calcareous shales and oil shales deposited in a quieter, more anoxic and stratified bottom water column (e.g. Sturn & Matter, 1978; Anadón & Utrilla, 1993). Therefore, this facies association is considered as having been deposited in an overall moderately deep lake environment in view of its tempo-spatial distribution in the basin (Figs 8–10).

Deep lake association

Description

This facies association is dominated by dark-coloured, well-laminated calcilutites (Figs 5J and 6G) and calcareous shales (Fig. 5K) intercalated with oil shales, locally with calcisiltite-calcilutites (Figs 8, 9 and 11). The features of these lithologies can be found in the documentation above and Tables 1 and 2. In comparison with the moderately deep facies association, this facies association is generally thinner and better laminated, with more abundant organic matter and in absence of bioturbations. These facies generally form the base of upward-coarsening successions deposited on the mid-lower slope and farther basinwards.

Interpretation

The dominance of dark-coloured, well-laminated calcilutites and calcareous shales absent of bioturbations suggests a persistent stratified and anoxic water-column in which they formed, with extremely rare interruption by low-density turbidity deposits (i.e. calcisiltite-calcilutites). This scenario may be analogous to that of modern lake Tanganyika, Africa, where the lake water is strongly stratified and permanently anoxic below depths of 150–250 m (Cohen, 1989, 1990; Huc *et al.*, 1990). The occurrence of this facies association (Figs 8–10) further supports a permanently quiescent, deep lake environment that allowed the accumulation of significant quantities of muddy sediments and organic matter.

SEQUENCE STRATIGRAPHIC FRAMEWORK OF THE CARBONATE UNIT

Although sequence stratigraphic methods were mainly applied to marine successions, they also have been successfully applied to non-marine

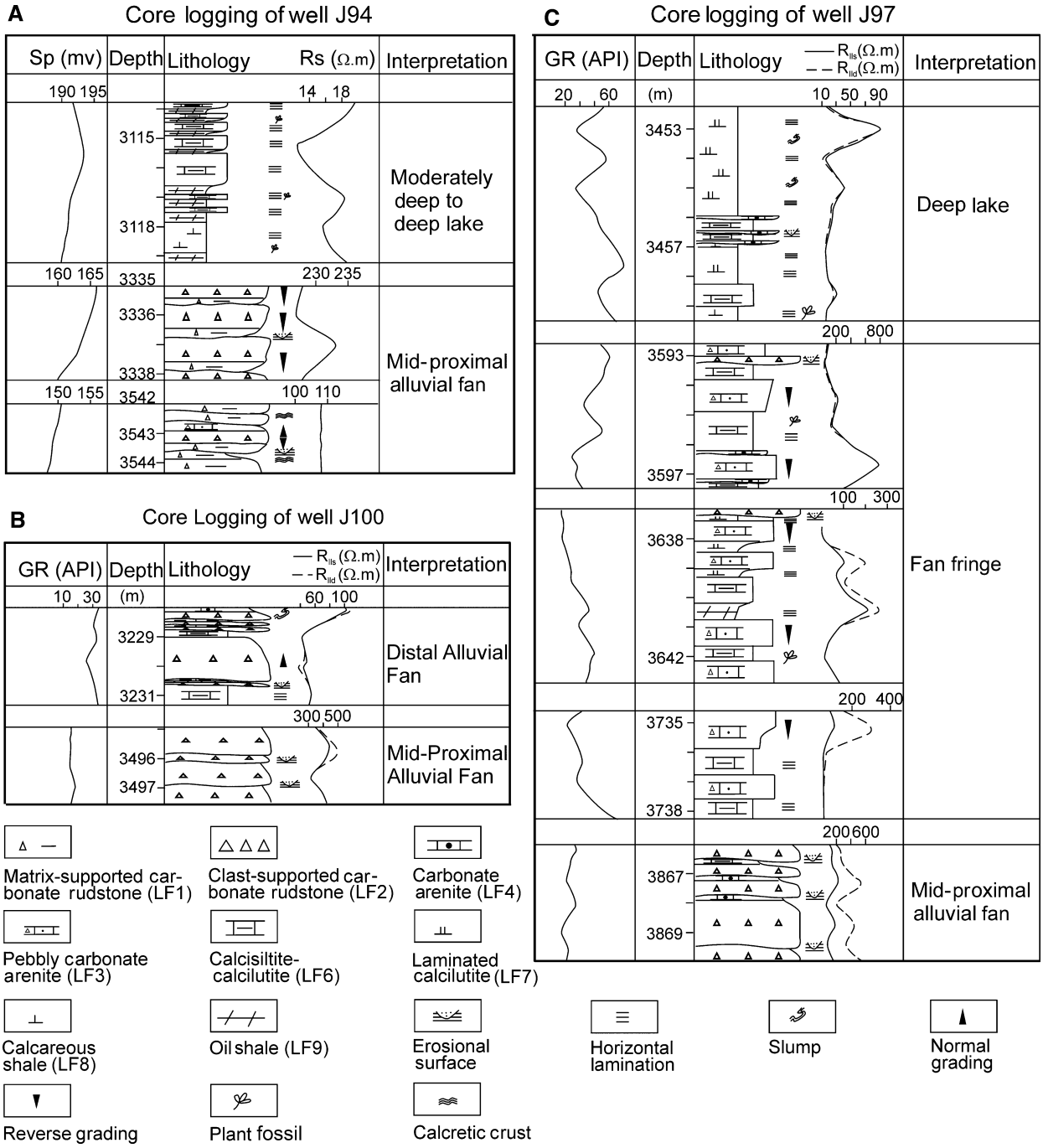

Fig. 11. Core logs from well J94 (A), well J100 (B) and well J97 (C), showing the distribution of lithologies from different facies associations in the lake. See Fig. 2 for well locations, Figs 8 and 9 for depositional setting.

lake deposits in continental rift and foreland basins (Scholz & Rosendahl, 1990; Liro, 1993; Bohacs *et al.*, 2000). Nevertheless, sequences and their depositional systems tracts that are formed in such lake basins are driven by local tectonic activity (i.e. block-tilting) and climate changes rather than by strictly eustatic sea-level changes (e.g. Contreras & Scholz, 2001). Therefore, the terms 'lowstand, transgressive and highstand' refer to the relative lake level changes rather than sea-level changes. Nevertheless, cautions should be always kept in mind when applying sequence stratigraphy to lake basins in view of the significant differences between marine and lake basins (Scholz *et al.*, 1998; Carrol & Bohacs, 1999; Bohacs *et al.*, 2000, 2003).

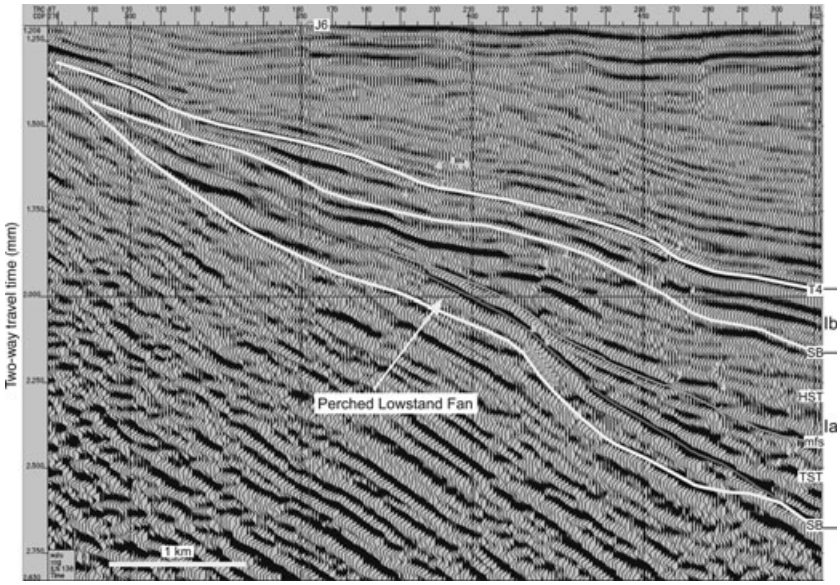

Fig. 12. Depositional dip section along seismic line (line 139) across well J6, including a valley-filling reflection pattern (perched fan) on the major Palaeozoic unconformity on the mid-upper slope. Note the lobate reflection patterns in HST. See Fig. 2 for the location.

Table 2. Mineral composition of fine-grained lake carbonates.

				Mineral composition (%)			
Sample	Well	Depth (m)	Lithofacies	Calcite	Dolomite	Clay mineral	Quartz
J94-1	J94	3114.20	Calcisiltite-calcilutite	86	3	5	6
J94-3		3118.71	Calcisiltite-calcilutite	85	3	6	6
J97-3	J97	3595.06	Calcisiltite-calcilutite	59	16	15	10
J97-5		3640.07	Calcisiltite-calcilutite	74	14	8	4
J97-6		3641.37	Calcisiltite-calcilutite	57	18	15	10
J97-7		3642.34	Calcisiltite-calcilutite	59	14	17	10
J97-8		3738.13	Calcisiltite-calcilutite	78	2	13	7
J100-1	J100	3228.94	Calcisiltite-calcilutite	59	29	6	6
J94-2	J94	3116.62	Laminated calcilutite	73	6	9	12
J97-1	J97	3454.00	Laminated calcilutite	62	22	5	11
J97-2		3455.75	Laminated calcilutite	52	5	24	14
J97-4		3638.49	Laminated calcilutite	73	15	8	4
J99-1	J99	2264.71	Calcareous shale	13	10	49	28
J99-2		2266.19	Calcareous shale	13	7	54	26
J99-3		2267.14	Calcareous shale	13	3	61	23
J99-4		2267.93	Calcareous shale	16	5	55	24

Analysed by semiquantitative X-ray diffraction.

In general, our seismic data exhibit an apparent divergent reflection pattern, particularly in the mid-lower part of the basin fill. Downlapping reflections and associated clinoform geometries resembling Gilbert delta megaforesets are scarce (Figs 4 and 7). These characters are analogous to the cases reported in modern, rapidly subsiding rift lake basins of Tanganyika and Malawi, Africa (Scholz & Rosendahl, 1990; Scholz *et al.*, 1998; Contreras & Scholz, 2001). Three large-scale depositional sequences (I–III), bounded by regional erosional unconformity surfaces (Figs 4 and 7), were identified in the overall Tertiary basin-fills (>3000 m thick), based on three-dimensional seismic reflection data and well logs; they are thus considered as second-order sequences next to the first-order sequence of the whole basin-filling sequence (according to definitions of Vail *et al.*, 1977). Sequence I starts from the basal Palaeozoic unconformity and ends at the top of Shahejie 2 Member, including Shahejie 3 and 2 Members. It consists mainly of the lower carbon-

ate successions and the upper siliciclastic successions (e.g. Fig. 8). Sequence II starts from the base of Shahejie 1 and ends at the top of Dongying Formation. Sequence III includes the Guantao and Minghuazhen formations. The latter two sequences are overwhelmingly composed of siliciclastic lacustrine deposits except for a minor amount of evaporites and carbonates in the base of the Shahejie 1 Member.

Based on seismic reflection termination patterns integrated with borehole data (well-logs, core samples and cutting fragments), two smaller-scale (herein the third order) sequences bounded by truncated reflections are identified in sequence I, namely sequences Ia and Ib (Figs 4, 7–9 and 12), in which the depositional systems tracts (cf. Van Wagoner *et al.*, 1988) are further recognized. The focus of this study is on the basal sequence (Ia), as sequence Ib is totally composed of siliciclastic lake deposits (Figs 8 and 9).

Within sequence Ia, six high-amplitude reflection intervals, indicators of a sharp lithological transition, can be further recognized (Fig. 7); they are constrained to the bounding surfaces of parasequence sets (Figs 8, 9 and 13) through forward stratigraphic modelling. However, several parasequence sets in the upper part of this sequence are not obvious in the seismic profile (compare Figs 7 and 8). The carbonate deposits are confined within the lower five time-line stratigraphic units, above which there are siliciclastic lake deposits. These parasequence sets generally consist of several smaller-scale, upward-coarsening parasequences with a fine-grained lithological base except for the basal rudstone packages (Fig. 13).

In sequence Ia, the mounded seismic facies on the basin floor (R1a, Figs 4 and 7), are composed of clastic (matrix- to clast-supported) carbonate rudstone packages with very limited lacustrine carbonates towards the basin centre (Figs 8 and 9), thus they are probably lowstand fan deposits. The palaeovalley fills on the mid-upper slope (R1b), localized between seismic lines 50–290 and CDPs 280–490 (Figs 7, 10A and 12; see Fig. 2 for location), extend axially along the basin, are onlapped by backstepped lobate seismic reflection patterns, and are also composed of matrix- and clast-supported carbonate rudstone packages (Figs 8 and 9). Based on these characteristics, they are interpreted as perched lowstand deposits within the palaeovalleys. The backstepped lobate bodies (R2–R4) mainly consist of clast-supported carbonate rudstones on the lake edge, passing lakewards into finer-grained lacustrine carbonate

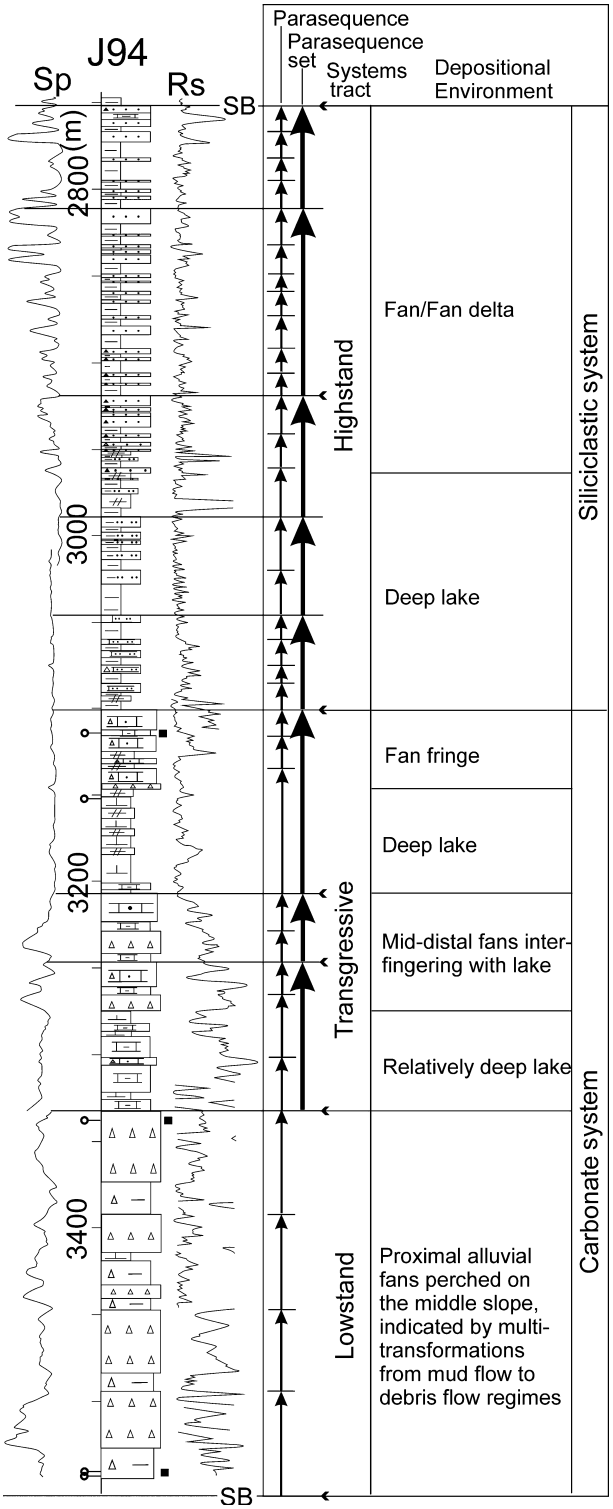

Fig. 13. Diagram showing vertical lithological variations of parasequences (thin arrows) and parasequence sets (thick arrows) in sequence Ia from well J94, interpreted from well-logs, core samples and cutting fragments and integrated with seismic data. Horizontal lines with arrows correspond to apparent high-amplitude reflectances in the seismic profile (see Fig. 7). Same legends as those in Figs 7 and 8.

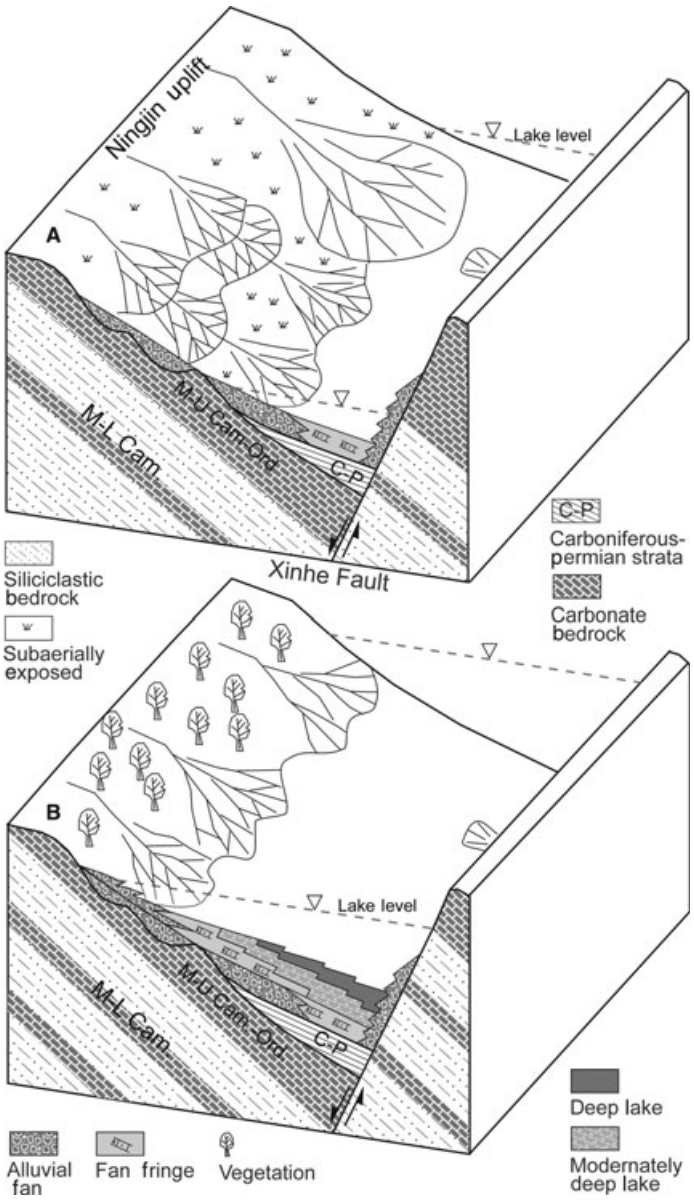

Fig. 14. Schematic diagram showing the spatial distribution and evolution of carbonate alluvial fan and lake systems and tectono-topographic setting during the early stage of basin filling in the middle segment of the Shulu Sag. (A) Carbonate alluvial fan and lake system during the lake lowstand stage. (B) Carbonate alluvial fan and lake system during the early transgressive stage.

deposits, i.e. calcilutites and calcareous shales (Figs 4, 7–9 and 10B); thus they probably represent lake transgressive fan deposits. These backstepped rudstone lobes are overlain by an extensive high-amplitude reflection (Figs 4, 7 and 12), which is dominated by siliciclastic mudstones/shales intercalated with subordinate siltstones. In the base, a thin layer consisting of oil shales is considered as the condensed section formed in response to the maximum flooding by lake water, which demarcates the transgressive and highstand deposits (Figs 8 and 9). The overlying highstand seismic facies is characterized by lobate reflection patterns (Figs 4 and 8), lithologically is dominated by fine-grained sandstone/mudstone siliciclastic deposits (Figs 8, 9 and 13). In this case, carbonate deposits are only present within the lower five time-equivalent stratigraphic horizons in the lowstand and transgressive deposits, i.e. in the base of Shahejie 3 Member (see Fig. 7).

EVOLUTION OF CARBONATE ALLUVIAL FAN-LAKE SYSTEMS

Carbonate deposition occurred both in the alluvial fan and profundal lake during the initial basin development, corresponding to the early stage of sequence Ia (Figs 4, 7–9 and 12). This

scenario is well constrained for the hinged western slope of the Shulu half-graben.

During the lake lowstand (or the initial basin-filling) stage and under intermediate climate conditions, carbonate alluvial fans occurred extensively on the lower slope of the western hinge, locally even reached the bottom of the slope very close to the eastern border-fault (Fig. 4), and only a narrow shallow lake belt was developed (Figs 4 and 10A). During this stage, alluvial fans were generally subaerial, particularly the mid-proximal fans (Fig. 14A; see earlier documentation). Some carbonate debris rudstones, however, stayed in the antecedent valley, localized between seismic lines 50–290 and CDPs 280–490, on the mid-upper slope (Figs 7, 8, 10A and 12). When debrisflows moved downslope through the valley, they were initially dammed and partially retained, and subsequently transported further down to bottom of the slope to form the alluvial fans (Fig. 14A). As such, the perched carbonate rudstones of debrisflow origin are approximately simultaneous with alluvial fans at the bottom of the slope, as described above.

During the lake transgressive (or deepening) stage, the climate tended to be more humid, leading to extensive vegetation in the catchment terrain as evidenced by the extensive presence of plant fossils in the fine-grained limestones. The lake expanded and deepened rapidly as the basin floor increasingly subsided as a result of more intense transtensional faulting and increased supply of water. During this stage, the carbonate alluvial fans tended to be smaller, narrow slope aprons along the basin edge (Figs 10B and 14B), which episodically backstepped updip and onlapped either upon the previous perched fan rudstone unit or upon the major Palaeozoic unconformity (Figs 4, 7 and 8). These carbonate alluvial fans discharged into the lake area where fan fringe, moderately deep and deep lake environments can be further differentiated (Figs 8, 9 and 10B). According to McPherson *et al.* (1987), these carbonate alluvial fans are fan-delta systems, as evidenced by upward-coarsening successions (or parasequences) (Figs 8 and 9). The carbonate deposits were sharply replaced by fine-grained siliciclastic deep lake deposits represented by shales intercalated with siltstones or fine-grained sandstones (Figs 8 and 9). The widespread occurrence of the dark/oil shale in the base of subsequent siliciclastic successions is considered as the condensed section during the maximum flooding of lake water. The highstand deposits are composed exclusively of siliciclastic fan-deltaic deposits (sandstones intercalated with shales/siltstones), commonly showing progradational lobes and upward-coarsening successions in vertical section (Figs 8, 9 and 13).

DISCUSSION

Tectonism and palaeotopography

The Shulu Sag was bounded by the NE–SW trending, Xinhe and Ningjin fault zones, within which several *en echelon* faults downthrowing to the north were terminated by the eastern Xinhe border fault generally at an acute angle (Fig. 2). This structural style points to a dextral transtensional faulting system, rather than a typical extensional faulting system, meaning a slight strike-slip probably occurred along the border faults (cf. Christie-Blick & Biddle, 1985). This scenario agrees with the dextral transtensional tectonics in Bohai Bay area, North China (Fig. 1; Hellinger *et al.*, 1985; Ye *et al.*, 1985; Zhang, 1985; Nábélek *et al.*, 1987; Zhou *et al.*, 2004). The bending in southern segments of the border faults is probably a reflection of the rotation around a vertical axis. However, the seismic profiles across the Shulu Sag reveal an apparent half-graben geometry (Figs 3, 4 and 7), suggesting that the block-fault tilting was still a major process in the basin formation, as being common for the extensional basins (Barr, 1987; Jackson *et al.*, 1988; Moretti & Colleta, 1988; Yielding, 1990). Extensive divergent seismic reflection patterns, with no apparent progradational clinoform and downlap reflections across the basin (Figs 4, 7 and 12), suggest a prolonged, rapid subsidence of the basin floor (within the hinged slope) (Scholz & Rosendahl, 1990; Scholz *et al.*, 1998) due to block-tilting. This created the abundant accommodation space available for the subsequent basin filling, which would have accelerated steepening of the hinged slope and deepening of the basin. These processes occurring during the basin filling, coupled with an intermediate to humid climate regime (see later discussion), enhanced the meromixis, anoxia and sediment starvation in the deep lake (e.g. Talbot, 1988; Cohen, 1989, 1990; Huc *et al.*, 1990).

The fault-block tilting and associated normal faulting have a major influence on the topography and the drainage basin geometry (size, slope length and gradient) of rift basins (e.g. Gawthorpe

et al., 1994). Although drainage basins developed on relatively gentle hangingwall slopes are generally larger and longer with a higher sediment supply compared with the footwall margin (e.g. Cohen, 1989, 1990; Scholz & Rosendahl, 1990; Soreghan & Cohen, 1996), no typical progradational fluvio-deltaic systems, as expected on the hangingwall slope in rift lake basins (Scholz *et al.*, 1998; Carrol & Bohacs, 1999; Bohacs *et al.*, 2000), occurred in our example. This is probably due to the relatively short length and rapidly subsiding, hinged slope. This scenario might have facilitated the formation of alluvial fans and/or fan deltas, rather than the formation of fluvio-deltaic systems, along the lake margin by debrisflows being drained from the catchment (cf. Hampton, 1972; Mulder & Alexander, 2001), allowing for further downslope sediment transport via gravity underflows. The relatively short distance between drainage basins and the depositional sites could have also reduced the duration of intense abrasion and dissolution of carbonate clasts into fine-grained carbonate grains and dissolved loads during transport (Gierlowski-Kordesch, 1998), thereby forming the coarse carbonate alluvial fan systems at the basin edge.

On the other hand, the relatively steep, hinged slope would have reduced reworking of coarse shoreline sediments into continuous beaches and shoreline bars by waves or longshore currents (cf. Cohen, 1990). The frequent downdip gravity flows being drained from the catchment area could have readily eroded the shoreline deposits deposited along the shoreline, when they passed by, which would be further re-moulded and redistributed sediments into the downward-moving gravity flows. Although shoreline bars and beaches are widely reported in modern and ancient lake examples (Cohen, 1989, 1990; Abrahão & Warme, 1990; Soreghan & Cohen, 1996), they, however, generally are poorly developed and of insufficient thickness and width to be recognized easily, particularly in seismic profiles and limited borehole controls (Scholz & Rosendahl, 1990; Bohacs *et al.*, 2000). These factors may account for the poorly constrained shoreline deposits in this study.

The antecedent topography prior to basin initiation also could have influenced the deposition in the basin, particularly during the early phase of basin filling. Based on numerous seismic profiles, two NE–SW trending palaeovalleys along the slope strike, filled with carbonate rudstones, were revealed on the mid-upper hangingwall homocline (Figs 7, 10A and 12). The axial-trending valleys could have partially dammed and retained the downward-moving debrisflows from the catchment, forming perched alluvial carbonate rudstones (Fig. 14A). The rest of the debrisflows would have moved downwards farther to the toe-of-slope to form the alluvial fans. Therefore, the perched alluvial rudstones and alluvial rudstones at the bottom of the basin floor were approximately deposited simultaneously only with a negligible difference in the timing of deposition. This interpretation is based mainly on the location and extension of the valleys. If the valleys extended downslope, they might be incised valleys, and no damming for the downslope-transporting debrisflows would have occurred. In this case, the palaeovalleys should be gradually onlapped by updip backstepped alluvial-lake systems. The fact that both the perched and basinal rudstones were onlapped progressively by the backstepped carbonate alluvial-lake systems (Figs 7, 8 and 12) excludes this possibility.

The WNW–ESE (or W–E) trending fault-controlled palaeo-relief (see Fig. 2B) could have influenced the hydrological circulation, i.e. the axial circulation of lake water, preventing the development of axial streams, particularly during the initial stage of basin filling (cf. Cohen, 1990; Liambiase, 1990). The elongated basin configuration with only a single opening to the north (Figs 1 and 2) may have restricted the water circulation, particularly on the southernmost corner. The semi-restricted circulation, on the other hand, may have enhanced stagnant and stratified lake waters, favouring formation of extensive fine-grained varve-like lithologies (e.g. laminated calcilutites and calcareous shales), and preservation of organic-rich facies in the lake.

Provenance

Lacustrine carbonates can occur in lake basins in the form of either autochthonous or allochthonous deposits under variable climatic conditions. In this study, the carbonate deposition in the early stage of basin-filling was strongly source-controlled, as demonstrated by the strong similarity of lithological and faunal compositions of lithoclasts (or grains) to those of Palaeozoic bedrocks beneath the catchment area. For example, the lithoclasts composed of edgewise conglomerates (Fig. 6D), interpreted as storm deposits in subtidal environments (Meng *et al.*, 1986, 1997; Shi *et al.*, 1997), extensively occur in

the Upper Cambrian carbonates in the North China platform (Ye, 1983; Meng *et al.*, 1997; Shi *et al.*, 1997). Variable dolostones are typically extensive in the Mid-Upper Ordovician (i.e. Majiagou Formation) in North China (Ye, 1983; Meng *et al.*, 1997). The marine fauna within lithoclasts, particularly those trilobites (Fig. 6B), are faunal associations typically from Cambro-Ordovician times (e.g. Ye, 1983; Zhang, 2003). These lines of evidence indicate that the carbonate lithoclasts were sourced from the surrounding Palaeozoic catchment, particularly the Mid-Upper Cambrian and Ordovician carbonate bedrocks. Weathered carbonate bedrocks from the Mid-Upper Cambro-Ordovician strata in uplifted terrains (Figs 3A and 14) could have provided both the clastic and dissolved carbonate loads to the Shulu Sag (e.g. Gierlowski-Kordesch, 1998). The coarse carbonate lithoclasts were transported through debris-flows and deposited in alluvial fans at the basin edge. Fine-grained clastic and dissolved carbonate loads were delivered further to the basin centre where fine-grained carbonates (calci-siltites, laminated calcilutites and calcareous shales; Figs 8, 9 and 14) were extensively deposited (or precipitated). The further uplift of Ningjin footwall block (the Xinhe footwall block as well), in response to progressive fault-block tilting (thereby basin subsiding), would have led to the denudation and erosion of deeper-buried Mid-Lower Cambrian bedrocks dominated by siliciclastics (Ye, 1983; Jiang *et al.*, 1996; Meng *et al.*, 1997; Shi *et al.*, 1997), providing significant siliciclastic influxes to the basin. In this case, siliciclastic alluvial fan/fan deltaic systems were developed, instead of carbonate alluvial fans in the lake, as observed here that the highstand deposits of sequence Ia and above sequences are overwhelmingly composed of siliciclastic fan/fan deltaic deposits (Figs 3, 8 and 9). Therefore, the lithology of catchment bedrock is the key factor controlling the development of carbonate alluvial fans and related lacustrine carbonates in the Shulu Sag.

Climate

Climate changes generally drive perturbations in hydrological circulation, thereby influencing the annual precipitation to evaporation ratios. Nevertheless, no clear correlation between climate change and lake deposits has been well established (Carrol & Bohacs, 1999; Bohacs *et al.*, 2003). Regional geological data show an apparent change from an arid to a semi-humid to humid climate occurred from the interval of the Shahejie 4 through Shahejie 3 in the context of lake expansion in central Hebei (Jizhong) area (Zhang *et al.*, 2001), during which temporary marine incursions might have occurred through unidentified channels. Marine incursion seems reasonable considering the presence of authigenic glauconite, marine fossils (i.e. foraminifera, bryozoans, sponges, echinoids, and marine species of ostracods, algae and nannofossils) in the equivalent strata (Wei & Xu, 1993). The connection with the open sea (i.e. Palaeo-East China Sea) to the east reconciles the timing of the global great marine transgression during the Early Eocene (cf. Haq *et al.*, 1987). Although marine fossils are not well constrained in the Shulu Sag, the presence of glauconite within this basin (a part of Jizhong Depression), as described earlier, is probably a reflection of marine influence during deposition. The presence of calcretes in the lowermost rudstone packages and plant fossils (leaf and wood) in the overlying fine-grained laminated limestones, and absence of evaporative minerals, as described earlier, indicate a transition of an intermediate to a semi-humid to humid climate, which was consistent with the regional to global climatic setting. This climatic regime is generally analogous to that of modern Lake Tanganyika and Malawi, East Africa where the climate is generally sub-humid (Cohen, 1989, 1990).

The semi-humid to humid climate, along with the accelerating subsidence of basin floor, could have favoured the formation of a meromictic, anoxic deep lake basin (Cohen, 1989, 1990; da Silva *et al.*, 2000). Under such a climate, with abundant precipitation and increased water supplies, there is an increased export of dissolved carbonate and nutrient loads from surrounding drainage terrains to the basin. A connection with marine basins, thereby increasing alkalinity and chemical stratification of lake water, could have induced a high bioproductivity in the surface water and anoxia in bottom waters (Bohacs *et al.*, 2000), which led to the deposition of well-laminated muddy limestone packages rich in organic matter in the central basin (Loftus & Greensmith, 1988; Talbot, 1988; Huc *et al.*, 1990). Accordingly, the occurrence of oil shales in the fine-grained, laminated carbonates suggests a higher primary productivity in surface water, probably in periods of a more humid climatic regime and a more expanded lake. Under these climatic conditions, more abundant precipitation could have carried more water and nutrient loads, but less

sediment loads and carbonate content (by dilution) to the basin due in part to denser vegetation (e.g. Einsele & Hinderer, 1998; Bohacs *et al.*, 2003), thereby resulting in a more significant rise in lake level (or lake expansion) and a closer connection with marine basins. These hydrological changes could have led to a more stable (thermal or chemical) stratification of lake waters, which, in turn, could have been extremely favourable for the production and preservation of organic matter (Bohacs *et al.*, 2000). This scenario is analogous to the formation of the Dinantian Oil Shales in the lacustrine Burdiehouse Limestone Formation of Scotland (Loftus & Greensmith, 1988).

Although the carbonate rudstones were mainly source-controlled (see the earlier discussion), the climate also played a role in their deposition. Prior to the basin initiation of the Shulu Sag (equivalent to the interval of Shahejie 4 or earlier), the climate was dry in Jizhong area (Zhang *et al.*, 2001), such that the mechanical weathering should have predominated over the drainage area. A shift to an intermediate climate at the onset of rapid subsidence of the hinged slope, and the associated increased rainfalls (mostly flash flooding), could have enhanced erosion of the sparsely vegetated drainage area and remoulded the weathered coarse carbonate particles and soils into debrisflows. The debrisflows ultimately would form the carbonate alluvial fans during lowstand lake level in the still restricted basin. As the climate tended to be more humid in the context of accelerating subsidence of the basin floor, persistent and sufficient precipitation would increase the volume of water, amount of dissolved sediments and nutrient loads due to enhanced chemical weathering, resulting in a progressive rise in lake level (lake transgression, and open to the Jizhong Depression). On the other hand, it would also lead to dense vegetation that acted as baffles and traps in the drainage area, as evidenced by the occurrence of plant fossils in lake deposits, and reduced sediment loads, including the coarse lithoclasts, to the basin (Einsele & Hinderer, 1998; Bohacs *et al.*, 2003). This scenario could have forced the alluvial fan-lake system episodically to backstep upon the hinged slope, as observed in the seismic profiles (Figs 4, 7 and 12). The occurrence of carbonate rudstone units thus probably reflects short-term climatic fluctuations back to a relatively dry climate in the context of a generally semi-humid to humid climate and basin deepening (lake transgression).

CONCLUSION

Shulu Sag is a NE–SW trending, elongate half-graben in central Hebei, North China, bordered by the Xinhe border fault to the east, and established on the hinged, western slope. Progressive subsidence as a result of fault-block tilting provided necessary accommodation space available for sediment and water accumulation below the basin's outlet.

Alluvial and lake carbonate deposits occur in the base of the Tertiary lake fills as lake lowstand and transgressive deposits of the basal sequence (Ia). During the lowstand stage and an intermediate climate, alluvial fans dominated by carbonate rudstones of debrisflows were localized on the lower portion of the hinged western slope, locally perched within palaeovalleys on the mid-upper slope; only a coeval narrow shallow lake belt occurred basinwards. During the transgressive stage and a semi-humid to humid climate, carbonate alluvial fans generally became smaller in size and backstepped updip upon the slope, as the lake greatly expanded and deepened. During this stage, the lake close to the border-fault zone was generally sediment-starved, characterized by a stratified and anoxic bottom lake water mass in the deep lake. Fine-grained laminated limestones (or calcareous shales) with intercalated oil shales were extensively deposited in the deep lake environment. During this stage, a connection to some extent with marine basins may have occurred due to the lake expansion coinciding with the global marine transgression.

The lithology of catchment bedrocks was the key cause for the carbonate deposition at the onset of the basin formation. The carbonate bedrock of the Mid-Upper Cambro-Ordovician in the catchment provided not only significant clastic, but also dissolved carbonate loads to the Shulu Sag, thereby forming thick alluvial and fine-grained lake carbonates there. However, the exhumation of the Mid-Lower Cambrian siliciclastics-dominated bedrocks finally terminated the carbonate deposition in the Shulu Sag due to significant siliciclastic influxes to the basin. A climatic transition from an intermediate to a semi-humid to humid climate led to denser vegetation in the drainage area, and more water and nutrient loads, but less clastic sediment loads to the basin, resulting in a meromictic, anoxic and starved deep lake. This case history indicates that the interactions between tectonics, provenance and climate fundamentally con-

trolled the carbonate deposition in this small half-graben.

ACKNOWLEDGEMENTS

Financial support from the Huabei (North China) Oil Company, CNPC allowed this study to be possible, from which further assistance was kindly provided during core logging and data collection. Partial support from the National Natural Science Foundation of China (grant no. 40372062 to D. C.) is sincerely acknowledged. Critical and constructive comments from E. H. Gierlowski-Kordesch, T. C. Blair, J. J. Liambiase and Editor I. Montañez greatly improved the manuscript.

REFERENCES

Abdul Aziz, H., Sanz-Rubio, E., Calvo, J., Hillgen, F. and **Krigsman, W.** (2003) Palaeoenvironmental reconstruction of a middle Miocene alluvial fan to cyclic shallow lacustrine depositional system in the Calatayud Basin (NE Spain). *Sedimentology*, **50,** 211–236.

Abrahão, D. and **Warme, J.E.** (1990) Lacustrine and associated deposits in a rifted continental margin–Campos Basin, offshore Brazil. In: *Laustrine Basin Exploration: Case Studies and Modern Analogs* (Ed. B.J. Katz), *AAPG Mem.*, **50,** 287–305.

Anadón, P. and **Utrilla, R.** (1993) Sedimentology and isotope geochemistry of lacustrine carbonates of the Oligocene Campins Basin, northeastern Spain. *Sedimentology*, **40,** 699–720.

Barr, D. (1987) Lithospheric stretching, detached normal faulting and footwall uplift. In: *Continental Extensional Tectonics* (Eds M.P. Coward, J.F. Dewey and P.L. Hancock), *Geol. Soc. Spec. Publ.*, **28,** 75–94.

Blair, T.C. (1999a) Cause of dominance by sheetflood vs. debris-flow processes on two adjoining alluvial fans, Death Valley, Californian. *Sedimentology*, **46,** 1015–1028.

Blair, T.C. (1999b) Sedimentology of debris-flow-dominated Warm Spring Canyon alluvial fan, Death Valley, Californian. *Sedimentology*, **46,** 941–965.

Bohacs, K.M., Carroll, A.R., Neal, J.E. and **Mankiewwicz, P.Z.** (2000) Lake-basin type, source potential, and hydrocarbon character: an integrated sequence-stratigraphic-geochemical framework. In: *Lake Basins through Space and Time* (Eds E.H. Gierlowski-Kordesch and K.R. Kelts), *AAPG Stud. Geol.*, **46,** 3–33.

Bohacs, K.M., Carroll, A.R. and **Neal, J.** (2003) Lessons from large lake systems – thresholds, nonlinearity, and strange attractions. In: *Extreme Depositional Environments: Mega End Members in Geologic Time* (Eds M.A. Chan and A.W. Archer), *Geol. Soc. Am. Spec. Pap.*, **370,** 75–90.

Carrol, A.R. and **Bohacs, K.M.** (1999) Stratigraphic classification of ancient lakes: balancing tectonic and climatic controls. *Geology*, **27,** 99–102.

Christie-Blick, N. and **Biddle, K.** (1985) Deformation and basin formation along strike-slip faults. In: *Strike-Slip Deformation, Basin Formation, and Sedimentation* (Eds K. Biddle and N. Christie-Blick), *SEPM Spec. Publ.*, **37,** 1–34.

Cohen, A.S. (1989) Facies relationships and sedimentation in large rift lakes and implications for hydrocarbon exploration: examples from lakes Turkana and Tanganyika. *Palaeogeogr. Palaeoclimat. Palaeoecol.*, **70,** 65–80.

Cohen, A.S. (1990) Tectono-stratigraphic model for sedimentation in Lake Tanganyika, Africa. In: *Lacustrine Basin Exploration: Case studies and Modern Analogs* (Ed. B.J. Katz), *AAPG Mem.*, **50,** 137–168.

Contreras, J. and **Scholz, C.H.** (2001) Evolution of stratigraphic sequences in multisegmented continental rift basins: models with the basins of the east African rift system. *AAPG Bull.*, **85,** 1561–1581.

Du, Y.H. (1990) Paleogene lacustrine carbonates and depositional models in Bohai Bay area. *Oil Gas Geol.*, **11,** 376–392 (in Chinese).

Du, Y.H. (1996) The Tertiary algal reefs in Shadong Province, North China. In: *The Ancient Organic Reefs of China and Their Relations to Oil and Gas* (Ed. J.S. Fan), pp. 275–293. Ocean Press, Beijing.

Einsele, G. and **Hinderer, M.** (1998) Quantifying denudation and sediment-accumulation systems (open and closed lakes): basic concepts and first results. *Palaeogeogr. Palaeoclimat. Palaeoecol.*, **140,** 7–21.

Esteban, M. and **Klappa, C.F.** (1983) Subaerial exposure environment. In: *Carbonate Depositional Environments* (Eds P.A. Scholle, D.G. Bebout and C.H. Moore), *AAPG Mem.*, **33,** 2–54.

Fisher, R.V. (1983) Flow transformation in sediment gravity flows. *Geology*, **11,** 273–274.

Gawthorpe, R.L., Fraser, A.J. and **Collier, R.E.L.I.** (1994) Sequence stratigraphy in active extensional basins: implications for the interpretation of ancient basin-fills. *Mar. Petrol. Geol.*, **11,** 642–658.

Gierlowski-Kordesch, E.H. (1998) Carbonate deposition in an ephemeral siliciclastic alluvial system: Jurassic Shuttle Meadow Formation, Newark Supergroup, Hartford Basin, USA. *Palaeogeogr. Palaeoclimat. Palaeoecol.*, **140,** 161–184.

Hampton, M.A. (1972) The role of subaqueous debris flow in generating turbidity currents. *J. Sed. Petrol.*, **42,** 775–793.

Haq, B.U., Hardenbol, J. and **Vail, P.R.** (1987) The chronology of fluctuating sea level since the Triassic. *Science*, **235,** 1156–1167.

Hellinger, S.J., Shedlock, K.M., Sclater, J.G. and **Ye, H.** (1985) The Cenozoic evolution of the North China Basin. *Tectonics*, **4,** 343–358.

Huc, A.Y., Le Fournier, J. and **Vandenbrouke, M.** (1990) Northern Lake Tanganyika – an example of organic sedimentation in an anoxic rift lake. In: *Laustrine Basin Exploration: Case Studies and Modern Analogs* (Ed. B.J. Katz), *AAPG Mem.*, **50,** 169–208.

Jackson, J.A., White, N.J., Garfunkel, Z. and **Anderson, H.** (1988) Relations between normal-fault geometry, tilting and vertical motions in extensional terrains: an example from the southern Gulf of Suez. *J. Struct. Geol.*, **10,** 155–169.

Jiang, M.S., Sha, Q.A. and **Liu, M.** (1996) Mixed siliciclastic-carbonates sediments in the Lower and Middle Cambrian, North China Platform. *Acta Sedimentol. Sinica*, **14** (Suppl.), 63–74.

Jin, Z.K., Zhou, Y.R., Zhang, X.X. and **Jiang, C.L.** (2002) Lacustrine carbonate sedimentary facies of the Shahejie Formation of Paleogene in Huanghua Depression. *J. Palaeogeogr.*, **4,** 11–18 (in Chinese).

Li, D.S. (1981) Geological structure and hydrocarbon occurrence of the Bohai Gulf oil and gas basin (China). In: *Petroleum Geology in China* (Ed. J.F. Mason), pp. 180–192. PennWell, Tulsa, OK.

Liambiase, J.J. (1990) A model for tectonic control of lacustrine stratigraphic sequences in continental rift basins. In: *Lacustrine Basin Exploration: Case Studies and Modern Analogs* (Ed. B.J. Katz), *AAPG Mem.*, **50,** 265–276.

Liro, L. (1993) Sequence stratigraphy of a lacustrine system: Upper Fort Union Formation (Paleocene), Wind River Basin, Wyoming, U.S.A. In: *Siliciclastic Sequence Stratigraphy: Recent Developments and Applications* (Eds P. Weimer and H.W. Posamentier), *AAPG Mem.*, **58,** 317–333.

Loftus, G.W. and **Greensmith, J.T.** (1988) The lacustrine Burdiehouse Limestone Formation – a key to the deposition of the Dinantian Oil Shales of Scotland. In: *Lacustrine Petroleum Source Rocks* (Eds A.J. Fleet, K. Kelts and M.R. Talbot), *Geol. Soc. Spec. Publ.*, **40,** 219–234.

Lowe, D.R. (1982) Sediment gravity flows: II. Depositional models with special reference to the deposits of high-density turbidity currents. *J. Sed. Petrol.*, **52,** 279–297.

Major, J.J. and **Iversion, R.M.** (1999) Debris-flow deposition: effects of pore-fluid pressure and frictional concentrated at flow margins. *Geol. Soc. Am. Bull.*, **111,** 1424–1434.

McPherson, J.G., Shanmugam, G. and **Moiola, R.J.** (1987) Fan-deltas and braid deltas: varieties of coarse-grained deltas. *Geol. Soc. Am. Bull.*, **99,** 331–340.

Meng, X.H., Qiao, X.F. and **Ge, M.** (1986) Study on ancient shallow sea carbonate storm deposits (tempestites) in North China and Dingjiatan-type facies model. *Acta Sedimentol. Sinica*, **4-2,** 1–18 (in Chinese).

Meng, X.H., Ge, M. and **Tucker, M.E.** (1997) Sequence stratigraphy, sea-level changes and depositional systems in the Cambro-Ordovician of the North China carbonate platform. *Sed. Geol.*, **114,** 189–222.

Miall, A.D. (1978) Lithofacies types and vertical profile model in braided river deposits: a summary. In: *Fluvial Sedimentology* (Ed. A.D. Miall), *Can. Soc. Petrol. Geol. Mem.*, **5,** 597–604.

Moretti, I. and **Colleta, B.** (1988) Fault-block tilting: the Gebel Zeit example, Gulf of Suez. *J. Struct. Geol.*, **10,** 9–19.

Mulder, T. and **Alexander, J.** (2001) The physical character of subaqueous sedimentary density flows and their deposits. *Sedimentology*, **48,** 269–299.

Nábélek, J., Chen, W.P. and **Ye, H.** (1987) The Tangshan earthquake and its implications for the evolution of the North China basin. *J. Geophys. Res.*, **92,** 12615–12628.

Nichols, G. and **Thompson, B.** (2005) Bedrock lithology control on contemporaneous alluvial fan facies, Oligo-Miocene, southern Pyrenees, Spain. *Sedimentology*, **52,** 571–585.

Nilsen, T.H. and **Sylvester, A.** (1995) Strike-slip basins. In: *Tectonics of Sedimentary Basins* (Eds C.J. Busby and R.V. Ingersoll), pp. 425–457. Blackwell Science, Oxford.

Odin, G.S. and **Matter, A.** (1981) De glauconiarum origine. *Sedimentology*, **28,** 611–641.

Platt, N.H. and **Wright, V.P.** (1992) Palustrine carbonates and the Florida everglades: towards an exposure index for the fresh-water environment? *J. Sed. Petrol.*, **62,** 1058–1071.

Qian, K., Du, Y.H., Zhou, S.X. and **Guan, S.R.** (1994) Lacustrine carbonates in China. In: *Sedimentology of China* (Eds Z.Z. Feng, Y.H. Wang, H.J. Liu and Q.A. Sha), pp. 153–179. Petroleum Industry Press, Beijing (in Chinese).

Scholz, C.A. and **Rosendahl, B.R.** (1990) Coarse-clastic facies and stratigraphic sequence models from Lakes Malawi and Tanganyika, East Africa. In: *Lacustrine Basin Exploration: Case Studies and Modern Analogs* (Ed. B.J. Katz), *AAPG Mem.*, **50,** 151–168.

Scholz, C.A., Moore, T.C., Jr, Hutchison, D.R., Golmshtok, A.J., Klitgord, K.D. and **Kurotchkin, A.G.** (1998) Comparative sequence stratigraphy of low-latitude versus high-latitude lacustrine rift basins: seismic data examples from the East Africa and Baikal rifts. *Palaeogeogr. Palaeoclimat. Palaeoecol.*, **140,** 401–420.

Shanmugan, G. (1996) High-density turbidity currents: are they sandy debris flows? *J. Sed. Res.*, **66,** 2–10.

Shi, X.Y., Chen, J.Q. and **Mei, S.L.** (1997) Cambrian sequence chronostratigraphic framework of the North China Platform. *China Univ. Geosci.*, **4,** 160–172 (in Chinese with English abstract).

da Silva, H.T., Caixeta, J.M., Magnavita, L.P. and **Sanches, C.P.** (2000) Syn-rift lacustrine deep-water deposits: examples from the Berriasian sandy strata of the Recôncavo Basin, northeastern Braizil. In: *Lake Basins through Space and Time* (Eds E.H. Gierlowski-Kordesch and K.R. Kelts), *AAPG Stud. Geol.*, **46,** 209–224.

Soreghan, M.J. and **Cohen, A.** (1996) Textural and compositional variability across littoral segments of Lake Tanganyika: the effect of asymmetric basin structure on sedimentation in large rift lakes. *AAPG Bull.*, **80,** 382–409.

Sturn, M. and **Matter, A.** (1978) Turbidites and varves in Lake Brienz (Switzerland): deposition of clastic detritus by density currents. In: *Modern and Ancient Lake Sediments* (Eds A. Matter and M.E. Tucker), *Int. Assoc. Sed. Spec. Publ.*, **2,** 147–168.

Szulc, J. and **Cwizewicz, M.** (1989) The lower Permian freshwater carbonates of the Slawkow Graben, southern Poland: sedimentary facies context and stable isotope study. *Palaeogeogr. Palaeoclimat. Palaeoecol.*, **70,** 107–120.

Talbot, M.R. (1988) The origins of lacustrine oil source rocks: evidence from the lakes of tropical Africa. In: *Lacustrine Petroleum Source Rocks* (Eds A.J. Fleet, K. Kelts and M.R. Talbot), *Geol. Soc. Spec. Publ.*, **40,** 29–43.

Tucker, M.E. and **Wright, V.P.** (1990) *Carbonate Sedimentology*. Blackwell Scientific, Oxford, 482 pp.

Vail, P.R., Mitchum, R.M.J., Todd, R.G., Widmier, J.M., Thompson, S., Sangree, J.B., Budd, J.N. and **Hatlelid, W.G.** (1977) Seismic stratigraphy and global changes of sea level, Part II. In: *Seismic Stratigraphy – Application to Hydrocarbon Exploration* (Ed. C.E. Payton), *Am. Assoc. Petrol. Geol. Mem.*, **26,** 49–212.

Van Wagoner, J.C., Posamentier, H.W., Mitchum, R.M., Vail, P.R., Sarg, J.F., Loutit, T.S. and **Hardenbol, J.** (1988) An overview of the fundamentals of sequence stratigraphy and key definitions. In: *Sea-level Changes: an Integrated Approach* (Eds C.K. Wilgus, B.S. Hastings, C.G.St.C. Kendall, H.P. Posamentier, C.A. Ross and J.C. Van Wagoner), *SEPM Spec. Publ.*, **42,** 39–45.

Wang, Y.H. (1983) Discovery and primary study of glauconite in modern lacustrine sediments from Fuxian Lake. *Chin. Sci. Bull.*, **28,** 1388–1392 (in Chinese).

Wei, K.S. and **Xu, H.D.** (1993) Palaeogene marine inundation in Jizhong (Central Hebei) area and its significance in sequence stratigraphy. *J. Grad. Sch. China Univ. Geosci.*, **7,** 274–284.

Weirich, F.H. (1988) Field evidence for hydraulic jumps in subaqeous sediment gravity flows. *Nature*, **332,** 626–629.

Yang, M.X., Liu, C.Y. and **Yang, B.Y.** (2001) Mesozoic tectonic transformation in Jizhong (central Hebei Province) Basin

and its petroleum geological implications. *Geotect. Geometal.*, **25,** 113–119 (in Chinese).

Ye, L.J. (1983) *Sedimentary Associations of the Northern China Platform*. Science Press, Beijing, 141 pp (in Chinese).

Ye, H., Shedlock, K.M., Hellinger, S.J. and **Sclater, J.G.** (1985) The North China Basin: an example of a Cenozoic rifted intraplate basin. *Tectonics*, **4,** 153–169.

Ye, D.Q., Zhong, X.C., Yao, Y.M., Yang, F., Zhang, S.B., Jiang, Z.X., Wang, Y.C., Sun, Z.C., Yang, S.Z., Zhao, X.L., Shen, H., Liang, H.D., Tang, W.S., Guan, X.T. and **Zhao, C.B.** (1993) *Tertiary System in Petroliferous Regions of China*, Vol. I: Introduction. Petroleum Industry Press, Beijing, 407 pp (in Chinese).

Yielding, G. (1990) Footwall uplift associated with Late Jurassic normal faulting in the northern North Sea. *J. Geol. Soc. Lond.*, **147,** 219–212.

Yuste, A., Luzón, A. and **Bauluz, B.** (2004) Provenance of Oligocene–Miocene alluvial and fluvial fans of the northern Ebro Basin (NE Spain): an XRD, petrographic and SEM study. *Sed. Geol.*, **172,** 251–268.

Zha, Q.H. (1988) Jizhong depression, China – its geologic framework, evolutionary history, and distribution of hydrocarbons. *AAPG Bull.*, **68,** 983–992.

Zhang, W.Y. (1985) *Tectonics of China and Adjacent Oceans and Continents*. Science Press, Beijing, 575 pp (in Chinese).

Zhang, W.T. (2003) Cambrian correlation between North America and China based on trilobite and conodont faunas. *Acta Palaeontol. Sinica*, **42,** 305–316.

Zhang, W.C., Cui, Z.Q., Han, C.Y., Guo, Y.J., Wang, H.S., Li, L., Wang, H.C. and **Li, X.P.** (2001) Basin evolution during Palaeogene and Petroleum potentials of Central Hebei (Jizhong) Depression. *J. Palaeogeogr.*, **3,** 45–54 (in Chinese).

Zhao, X.F. and **Tang, Z.H.** (2000) Lacustrine deposits of the Upper Permian Pidingquan Formation in the Kelameili area of the Junggar Basin, Xingjiang, China. In: *Lake Basins through Space and Time* (Eds E.H. Gierlowski-Kordesch and K.R. Kelts), *AAPG Stud. Geol.*, **46,** 111–122.

Zhou, Y.Q., Zhou, L.Q. and **Guo, Y.F.** (2004) *Petroleum Geology of Cenozoic Basins, Eastern China*. Petroleum Industry Press, Beijing, 355 pp (in Chinese).

Zhu, H., Chen, Y. and **Pu, P.** (1989) *Environments and Sedimentation of Fault Lakes, Yunnan Province*. Science Press, Beijing, 513 pp (in Chinese).

Manuscript received 8 July 2005; revision accepted 23 August 2006